SLAC-PUB-10972

Order-Disorder Transitions in Cross-linked Block Copolymer Solids

Jayajit Das,[1,*] Hyeok Hahn,[1,*] Nitash P. Balsara,[1,†]

Arup K. Chakraborty,[1,2,3,†] and John A. Pople[4]

[1]*Department of Chemical Engineering and Materials Science Division,*

Lawrence Berkeley National Laboratory,

University of California, Berkeley, California 94720

[2]*Department of Chemistry, University of California, Berkeley, California 94720*

[3]*Physical Biosciences Division, Lawrence Berkeley National Laboratory,*

University of California, Berkeley, California 94720

[4]*Stanford Synchrotron Laboratory, SLAC,*

PO Box 4349, Stanford, California 94309

(Dated: May 7, 2003)

Work supported in part by the Department of Energy contract DE-AC02-76SF00515

Abstract

With a view toward creating solid block copolymers wherein the order-disorder transition can be accessed many times we investigate the nature of order-disorder transitions in cross-linked diblock copolymer melts using synergistic theory and experiment. A mean-field theory based on a coarse grained free-energy and the Random Phase Approximation (RPA) is developed for the system of interest. The quenched distribution of cross-links is averaged using the replica method. The phase behavior of a particular A-B block copolymer melt with a randomly cross-linked B-block is determined as a function of the Flory-Huggins interaction parameter (χ) and the average number of cross-links per chain N_c. We find for a cross-link density greater than N_c^* the B monomers are localized within a region of size $\xi \sim (N_c - N_c^*)^{-1/2}$. The cross-links strongly oppose ordering in the system as ξ becomes comparable to the radius of gyration of the block copolymer chain. As such the order-disorder transition temperature T_{ODT} decreases precipitously when $N_c > N_c^*$. When $N_c < N_c^*$, T_{ODT} increases weakly with N_c. Experiments were conducted on cross-linked polystyrene-block-polyisoprene copolymer samples wherein the polyisoprene block was selectively cross-linked at a temperature well above the order-disorder transition temperature of the pure block copolymer. Small angle X-ray scattering (SAXS) and birefringence measurements on the cross-linked samples are consistent with the theoretical prediction. T_{ODT} decreases rapidly when the cross-linking density exceeds the critical cross-linking density.

*The first two authors contributed equally to the paper

†Corresponding author

I. INTRODUCTION

The fact that molten block copolymers undergo reversible order-disorder transitions is well-established [1, 2]. In the ordered state, the blocks are microphase separated into structures with either crystalline (e.g. spheres arranged on a body centered cubic lattice) or liquid crystalline (e.g. cylinders arranged on a hexagonal lattice) symmetry. In the disordered state, block copolymers are isotropic liquids. Microphase separation of block copolymers is exploited in a number of practical applications such as thermoplastic elastomers and adhesives [3, 4, 5, 6]. In these traditional applications, the microphase separation transition is used once during the life time of the product - the material is processed in the isotropic (liquid) state and used in the ordered (soft solid) state. Our objective is to create solid block copolymer materials wherein the order-disorder transition is accessed numerous times during the life-time of the product. This would enable the use of block copolymers in new applications that rely on reversible changes in the mechanical properties of solids such as shape memory, actuators, and artificial muscles[7, 8, 9, 10]. The possibility of using cross-linked networks in such applications was recognized long ago [11]. Polymer networks immersed in solvents can swell and shrink reversibly is response to changes in thermodynamic potentials such as solvent quality, pH, etc. [11, 12, 13]. It has proven difficult to exploit the swelling of elastomers in practical applications (e.g. artificial muscles) due to two reasons: (1) the large changes in sample volume lead to fatigue and eventual degradation of mechanical integrity, and (2) the kinetics of the phase transition is slow because it is limited by the diffusion of solvent in and out of the material [14]. It is thus desirable to design solids wherein changes in material properties do not require changes in volume or diffusion across macroscopic dimensions.

Cross-linking reactions have been used to create a variety of polymeric nanostructures. Block copolymer micelles with cross-linked shells are being considered for use as drug delivery vehicles [15, 16, 17, 18]. Macromolecules with novel architectures such as worm-like and mushroom-like structures have been produced by a combination of block copolymer self-assembly and cross-linking [19, 20, 21]. Periodic structures formed in block copolymers and their blends have been stabilized by cross-linking [22, 23]. These cross-linked structures have been used as templates for preparing nanostructured inorganic materials [24, 25]. The objective of these studies [15, 16, 17, 18, 19, 20, 21, 22, 23, 24, 25] was to "fix" the

nanostructures.

Our objective is to create cross-linked nanostructures that disassemble and reform spontaneously and reversibly in response to changes in temperature. We begin with a melt of a linear polystyrene-polyisoprene diblock copolymer that exhibits an ordered phase composed of polystyrene cylinders arranged on a hexagonal lattice in a polyisoprene matrix. The ordered phase melts into a disordered liquid when heated above 114°C. We added a cross-linking agent to the block copolymer and conducted the cross-linking reaction at 160°C, i.e. in the disordered state. The cross-linking agent used in this study selectively cross-links the polyisoprene chains. Synergistic theoretical and experimental work was conducted to elucidate the phase behavior of these cross-linked systems.

We derive coarse grained free energy for cross-linked diblock copolymer melts. The cross-links are treated as a permanent quenched disorder following the method of Deam and Edwards [26]. We resort to the replica method in order to average over the cross-links. The Random Phase Approximation (RPA) [2, 27] is employed to evaluate the free energy as an expansion in powers of the density variables. This enables determination of the order-disorder transition temperature of our system as a function of cross-linking density. Experimental characterization of our cross-linked block copolymers was based on swelling data, optical birefringence, and small angle X-ray scattering (SAXS). Our initial experimental findings are reported in ref. [28]. The article is organized as follows : In Sec. IIA we introduce the model and derive the coarse grained free energy. The mean field analysis and the phase diagram are presented in Sec. IIB. Details of the calculations for Sec. II are provided in the Appendices. The experimental details (SAXS and Birefringence) are given in Sec. III. In the next section (Sec. IV) we discuss the results of the experiments and compare that with the analytical calculations. Conclusions are offered in Sec. V.

II. THEORY

A. The Free energy

Consider a polymer melt of volume V with m copolymer chains, each of which consists of N monomers with volume fraction f between the A (polystyrene (PS)) and B (polyisoprene (PI)) blocks. The energy of the system is given by the standard Edwards Hamiltonian

[29, 30] :

$$H/k_BT = \sum_{i=1}^{m} \frac{3}{2Nl_0^2} \int_0^1 ds \left(\frac{d\mathbf{r}_i}{ds}\right)^2 + V(\{\mathbf{r}_i\}) \,, \tag{1}$$

where $\{\mathbf{r}_i\}$ describes the configuration of the ith chain in 3D, l_0 is the persistence length (Kuhn length) and the excluded volume interactions between monomers are described by,

$$V(\{\mathbf{r}_i\}) \;=\; \sum_{i,j=1}^{m} \sum_{a,b=1}^{2} \frac{v_{ab}N^2}{2} \int_a ds \int_b ds' \delta(\mathbf{r}_i(s) - \mathbf{r}_j(s')) \,, \tag{2}$$

where v_{11}, v_{22} and v_{12} are the strengths of couplings between A-A, B-B and A-B monomers and $\int_1 \equiv \int_0^f$ and $\int_2 \equiv \int_f^1$. The Flory-Huggins parameter [1, 27] $\chi = (v_{12} - (v_{11} + v_{22})/2)v^{-1}$, where v is the average monomer volume. Phenomenologically χ [31] varies with the temperature as $\chi = a + b/T$, where a and b are system dependent parameters. In the experiments [28] the polyisoprene segments are cross-linked in the disordered phase by using dicumyl peroxide (DCP). However first we consider the general case with cross-links between A-A, B-B and A-B and later we focus on the experimentally relevant case where only the B-B type of cross-links are present in the system. If there are R_{11}, R_{22} and R_{12} permanent cross-links between A-A, B-B and A-B respectively, the probability a particular realization of a certain type (A-A, B-B or A-B) of cross-links can be expressed by the Deam-Edwards form [26]. The constraint due to the lth cross-link between the segment s_l of chain i_l and the segment s_l' of chain i_l' is described by $\delta(\mathbf{r}_{i_l}(s_l) - \mathbf{r}_{i_l'}(s_{i_l}'))$. Thus the probability distribution for a particular cross-link configuration $\{\mathbf{r}_{i_l}(s_l); \mathbf{r}_{i_l'}(s_l')\}$ is given by

$$P_{ab}(\{\mathbf{r}_{i_l}(s_l); \mathbf{r}_{i_l'}(s_l')\}) \propto \prod_{l=1}^{R_{ab}} \delta(\mathbf{r}_{i_l}(s_l) - \mathbf{r}_{i_l'}(s_l')) \,, \tag{3}$$

where $a = \{1, 2\}$, $b = \{1, 2\}$ and $\langle \cdots \rangle$. The set of cross-linked segments $\{\mathbf{r}_{i_l}(s_l); \mathbf{r}_{i_l'}(s_l')\}$ is drawn from the equilibrium configurations in order to eliminate the vast number of cross-linked configurations which correspond to unphysical conformations of the chains [26, 32]. Instead of using the distribution with fixed number of cross-links it will turn out to be convenient to carry out calculations later if the total number of cross-links is allowed to fluctuate around the mean in a quasi-Poisson manner [33, 34]. The probability distribution after the inclusion of the fluctuations in the total number of cross-links can be described by,

$$P_{ab}(\{\mathbf{r}_{i_l}(s_l); \mathbf{r}_{i_l'}(s_l')\}) = \frac{\mathcal{N}_{ab}^{-1}}{R_{ab}!} \left(\frac{\mu_{ab}^2 V}{2m}\right)^{R_{ab}} \prod_{l=1}^{R_{ab}} \delta(\mathbf{r}_{i_l}(s_l) - \mathbf{r}_{i_l'}(s_l')). \tag{4}$$

The parameters $\{\mu_{ab}\}$ determine the average number of cross-links per macromolecule in the following manner : $\mu_{11}^2 f^2/2 \approx R_{11}/m$, $\mu_{12}^2 f(1-f) \approx R_{12}/m$ and $\mu_{22}^2 (1-f)^2/2 \approx R_{22}/m$. The normalization factor $\mathcal{N}_{ab}$ is given by

$$\begin{aligned}\mathcal{N}_{ab} &= \sum_{R_{ab}=1}^{\infty} \sum_{l=1}^{R_{ab}} \sum_{i_l=1}^{m} \sum_{i'_l=1}^{m} \frac{1}{R_{ab}!} \left(\frac{\mu_{ab}^2 V}{2m}\right)^{R_{ab}} \left\langle \prod_{l=1}^{R_{ab}} \int_a ds_l \int_b ds'_l \delta(\mathbf{r}_{i_l}(s_l) - \mathbf{r}_{i'_l}(s'_l)) \right\rangle \\ &= \left\langle \exp\left[\left(\frac{\mu_{ab}^2 V}{2m}\right) \sum_{i,j=1}^{m} \int_a ds \int_b ds' \, \delta(\mathbf{r}_i(s) - \mathbf{r}_j(s')) \right] \right\rangle .\end{aligned} \tag{5}$$

$\langle \cdots \rangle$ denotes average over configurations with the Boltzmann weight $e^{-\beta H}$ ($\beta = (k_B T)^{-1}$). The free-energy F of the system, averaged over the cross-link distribution can be expressed as,

$$F \;=\; -\beta^{-1} \int \mathcal{D}[\mathbf{r}_i(s)] \prod_{a,b=1}^{2} \left[\sum_{R_{ab}=1}^{\infty} \sum_{l=1}^{R_{ab}} \sum_{i_l=1}^{m} \sum_{i'_l=1}^{m} \int_a ds_l \int_b ds'_l \, P_{ab}(\{\mathbf{r}_{i_l}(s_l); \mathbf{r}_{i'_l}(s'_l)\}) \right] \ln Z \,, \tag{6}$$

where

$$Z = \int \mathcal{D}[\mathbf{r}_i(s)] e^{-\beta H} \prod_{a,b=1}^{2} \prod_{l=1}^{R_{ab}} \delta(\mathbf{r}_{i_l}(s_l) - \mathbf{r}_{i'_l}(s'_l)) \tag{7}$$

In order to evaluate the average of $\ln Z$ over the realizations of cross-links we employ the replica trick [26, 35, 36]. The structure of Eq. (6) allows us to consider the system as a collection of $n+1$ replicas where the additional 0th replica system generates the cross-link distribution described by Eq. (4). The free-energy F can be obtained from the identity,

$$F = -\beta^{-1} \lim_{n \to 0} \frac{\mathcal{Z}_{n+1} - \mathcal{Z}_1}{n \mathcal{Z}_1} \,, \tag{8}$$

where $\mathcal{Z}_{n+1}$ is defined as

$$\begin{aligned}\mathcal{Z}_{n+1} \;=\; \int \mathcal{D}[\mathbf{r}_i^{\alpha}(s)] \exp\Bigg[-\sum_{\alpha=0}^{n} \left\{ \sum_{i=1}^{m} \frac{3}{2Nl_0^2} \int_0^1 ds \left(\frac{d\mathbf{r}_i^{\alpha}}{ds}\right)^2 + V(\{\mathbf{r}_i^{\alpha}\}) \right\} + \\ \sum_{a,b=1}^{2} \frac{\mu_{ab}^2 V}{2m} \sum_{i,j=1}^{m} \int_a ds \int_b ds' \prod_{\alpha=0}^{n} \delta(\mathbf{r}_i^{\alpha}(s) - \mathbf{r}_j'^{\alpha}(s')) \Bigg] .\end{aligned} \tag{9}$$

In the above equation $\{\mathbf{r}_i^{\alpha}\}$ refers to the polymer configuration in the α th replica system. The index α runs from 0 to n implying average over $n+1$ replica copies of the system. Note

that the cross-links induce coupling between different replica systems which is reflected in Eq. (9). Now we will focus on the experimentally relevant case [28] with only B-B (polyisosprene-polyisosprene) type cross-links present in the system. We denote μ_{22} by μ in all further calculations from now. In order to investigate the equilibrium phases of the system we construct (Appendix A) a coarse grained free-energy as a functional of the densities of A and B monomers using the Random Phase Approximation (RPA) [27]. RPA works remarkably well for polymer melts [2, 37] where density fluctuations are weak. The density variables for the monomers A and B are defined as,

$$\rho_A^\alpha(\mathbf{r}^\alpha) = \sum_{i=1}^{m} \int_0^f ds\, \delta(\mathbf{r}^\alpha - \mathbf{r}_i^\alpha(s)) \tag{10}$$

and

$$\rho_B^\alpha(\mathbf{r}^\alpha) = \sum_{i=1}^{m} \int_f^1 ds\, \delta(\mathbf{r}^\alpha - \mathbf{r}_i^\alpha(s)) \tag{11}$$

respectively. One can introduce $3(n+1)$ dimensional vectors, such as $\hat{\mathbf{x}} \equiv \{\mathbf{x}_0, \mathbf{x}_1, \mathbf{x}_2, \cdots, \mathbf{x}_n\}$ to express the coupling between the replica copies due to cross-links in a compact form [33, 38]. We define density variables $\rho_A(\hat{\mathbf{r}})$ and $\rho_B(\hat{\mathbf{r}})$ as

$$\rho_A(\hat{\mathbf{r}}) \;=\; \sum_{i=1}^{m} \int_0^f ds \prod_{\alpha=0}^{n} \delta(\mathbf{r}^\alpha - \mathbf{r}_i^\alpha(s)) = \sum_{i=1}^{m} \int_0^f ds\, \delta(\hat{\mathbf{r}} - \hat{\mathbf{r}}_i(s)) \tag{12}$$

and

$$\rho_B(\hat{\mathbf{r}}) \;=\; \sum_{i=1}^{m} \int_f^1 ds \prod_{\alpha=0}^{n} \delta(\mathbf{r}^\alpha - \mathbf{r}_i^\alpha(s)) = \sum_{i=1}^{m} \int_f^1 ds\, \delta(\hat{\mathbf{r}} - \hat{\mathbf{r}}_i(s)), \tag{13}$$

which allows us to write the last term in the free energy (Eq. (9)) as $(\mu^2 V/2m) \int d\hat{\mathbf{r}} \rho_B(\hat{\mathbf{r}}) \rho_B(\hat{\mathbf{r}})$. This form is similar to the excluded volume interaction $-\chi v N^2 \int d\mathbf{r} [\rho_A(\hat{\mathbf{r}})\rho_A(\hat{\mathbf{r}}) + 2\rho_A(\hat{\mathbf{r}})\rho_B(\hat{\mathbf{r}}) + \rho_B(\hat{\mathbf{r}})\rho_B(\hat{\mathbf{r}})]$ in di-block copolymers. The variables $\rho_{A,B}^\alpha(\mathbf{r}^\alpha)$ and $\rho_{A,B}(\hat{\mathbf{r}})$ are not independent but are related to each other as,

$$\rho_{A,B}^\alpha(\mathbf{r}^\alpha) = \int d\hat{\mathbf{x}} \rho_{A,B}(\hat{\mathbf{x}}) \delta(\mathbf{x}^\alpha - \mathbf{r}^\alpha)\,. \tag{14}$$

In Fourier space the above relation translates to

$$\rho_{A,B}^\alpha(\mathbf{k}^\alpha) = \rho_{A,B}(\mathbf{0}, \cdots \mathbf{0}, \mathbf{k}^\alpha, \mathbf{0} \cdots, \mathbf{0}) \tag{15}$$

where $\rho_{A,B}(\mathbf{k}^0, \mathbf{k}^1, \cdots \mathbf{k}^\alpha, \cdots \mathbf{k}^n) \equiv \rho_{A,B}(\hat{\mathbf{k}})$ are the Fourier transforms of $\rho_{A,B}(\hat{\mathbf{r}})$ defined as

$$\rho_{A,B}(\hat{\mathbf{k}}) = \int d\hat{\mathbf{r}}\ e^{i\hat{\mathbf{k}}\cdot\hat{\mathbf{r}}}\rho_{A,B}(\hat{\mathbf{r}})\,. \tag{16}$$

It is useful to decompose $\rho_A(\hat{\mathbf{k}})$ and $\rho_B(\hat{\mathbf{k}})$ in different replica sectors to provide a clear physical interpretation. We adopt the same decomposition scheme used by Goldbart et. al [33] in dealing with cross-linked homopolymer systems. According to that scheme the variable $\rho_A(\hat{\mathbf{k}})$ can be split in the following manner.

$$\begin{aligned}\rho_A(\hat{\mathbf{k}}) &= \rho_A(\hat{\mathbf{k}})\delta_{\hat{\mathbf{k}},0} + \left(\sum_{\alpha=0}^{n}\prod_{\beta=0,\beta\neq\alpha}^{n}\delta_{\mathbf{k}^\beta,0}\right)(1-\delta_{\hat{\mathbf{k}},0})\rho_A(\hat{\mathbf{k}}) + \left(1-\sum_{\alpha=0}^{n}\prod_{\beta=0,\beta\neq\alpha}^{n}\delta_{\mathbf{k}^\beta,0}\right)(1-\delta_{\hat{\mathbf{k}},0})\rho_A(\hat{\mathbf{k}}) \\ &= (\rho_A)_0 + (\rho_A)_1 + \bar{\rho}_A \end{aligned} \tag{17}$$

The first term $(\rho_A)_0$ in Eq. (17) is non-zero when all the elements in $\{\mathbf{k}^\alpha\}$ are zero and we can say that $(\rho_A)_0$ belongs to the zero replica sector. The second term $(\rho_A)_1$ would fall in the one replica sector where all but one of $\{\mathbf{k}^\alpha\}$ is zero. $(\rho_A)_1$ would denote the variable $\rho_A^\alpha(\mathbf{k}^\alpha)$ which is the density in the α-th replica system. The last term $\bar{\rho}_A$ resides in the higher replica sector where more than one of the $\{\mathbf{k}^\alpha\}$ are non-zero. The presence of a non-zero higher replica sector in $\rho_A(\hat{\mathbf{k}})$ would reflect coupling between different replica systems. Now we set out to study the ordering transition in the cross-linked diblock copolymer melt by using the above variables and decomposition scheme.

In block copolymer systems the microphase segregation transition is described by the order parameter

$$\psi^\alpha(\mathbf{r}^\alpha) = (1-f)\rho_A^\alpha(\mathbf{r}^\alpha) - f\rho_B^\alpha(\mathbf{r}^\alpha)\,. \tag{18}$$

The above definition makes $\int d\mathbf{r}^\alpha\psi^\alpha(\mathbf{r}^\alpha) = 0$ or in fourier space $\psi^\alpha(\mathbf{k}^\alpha = 0) = 0$. $\langle\psi^\alpha(\mathbf{r}^\alpha)\rangle$ is finite when the system undergoes a transition from the disordered state to the ordered state. If we assume the system is incompressible, which is a very good approximation for polymer melts [2, 37], the total density is a constant throughout the sample and can be written as

$$c^\alpha(\mathbf{r}^\alpha) = \rho_A^\alpha(\mathbf{r}^\alpha) + \rho_B^\alpha(\mathbf{r}^\alpha) = \frac{m}{V}\,. \tag{19}$$

The variables $\psi(\hat{\mathbf{r}})$ and $c(\hat{\mathbf{r}})$ are defined as $\psi(\hat{\mathbf{r}}) = (1-f)\rho_A(\hat{\mathbf{r}}) - f\rho_B(\hat{\mathbf{r}})$ and $c(\hat{\mathbf{r}}) = \rho_A(\hat{\mathbf{r}}) + \rho_B(\hat{\mathbf{r}})$. $\psi(\hat{\mathbf{k}})$ obeys the constraint $\psi(\hat{\mathbf{k}} = 0) = 0$. The free-energy F of the system can be calculated using the RPA (Appendix A) which to fourth order in ψ and c is given by,

$$\beta F[\psi,c] = \int_{\hat{\mathbf{k}}} \left[\Gamma^{(2)}_{\psi\psi}\psi(\hat{\mathbf{k}})\psi(-\hat{\mathbf{k}}) + \Gamma^{(2)}_{\psi c}\psi(\hat{\mathbf{k}})c(-\hat{\mathbf{k}}) + \Gamma^{(2)}_{cc}c(\hat{\mathbf{k}})c(-\hat{\mathbf{k}})\right] +$$
$$\int_{\hat{\mathbf{k}}_1,\hat{\mathbf{k}}_2} \left[\Gamma^{(3)}_{\psi\psi\psi}\psi(\hat{\mathbf{k}}_1)\psi(\hat{\mathbf{k}}_2)\psi(-\hat{\mathbf{k}}_1-\hat{\mathbf{k}}_2) + \Gamma^{(3)}_{\psi\psi c}\psi(\hat{\mathbf{k}}_1)\psi(\hat{\mathbf{k}}_2)c(-\hat{\mathbf{k}}_1-\hat{\mathbf{k}}_2) +\right.$$
$$\left.\Gamma^{(3)}_{\psi cc}\psi(\hat{\mathbf{k}}_1)c(\hat{\mathbf{k}}_2)c(-\hat{\mathbf{k}}_1-\hat{\mathbf{k}}_2) + \Gamma^{(3)}_{ccc}c(\hat{\mathbf{k}}_1)c(\hat{\mathbf{k}}_2)c(-\hat{\mathbf{k}}_1-\hat{\mathbf{k}}_2)\right] +$$
$$\int_{\hat{\mathbf{k}}_1,\hat{\mathbf{k}}_2,\hat{\mathbf{k}}_3} \left[\Gamma^{(4)}_{\psi\psi\psi\psi}\psi(\hat{\mathbf{k}}_1)\psi(\hat{\mathbf{k}}_2)\psi(\hat{\mathbf{k}}_3)\psi(-\hat{\mathbf{k}}_1-\hat{\mathbf{k}}_2-\hat{\mathbf{k}}_3) +\right.$$
$$\Gamma^{(4)}_{\psi\psi\psi c}\psi(\hat{\mathbf{k}}_1)\psi(\hat{\mathbf{k}}_2)\psi(\hat{\mathbf{k}}_3)c(-\hat{\mathbf{k}}_1-\hat{\mathbf{k}}_2-\hat{\mathbf{k}}_3) + \Gamma^{(4)}_{\psi\psi cc}\psi(\hat{\mathbf{k}}_1)\psi(\hat{\mathbf{k}}_2)c(\hat{\mathbf{k}}_3)c(-\hat{\mathbf{k}}_1-\hat{\mathbf{k}}_2-\hat{\mathbf{k}}_3) +$$
$$\left.\Gamma^{(4)}_{\psi ccc}\psi(\hat{\mathbf{k}}_1)c(\hat{\mathbf{k}}_2)c(\hat{\mathbf{k}}_3)c(-\hat{\mathbf{k}}_1-\hat{\mathbf{k}}_2-\hat{\mathbf{k}}_3) + \Gamma^{(4)}_{cccc}c(\hat{\mathbf{k}}_1)c(\hat{\mathbf{k}}_2)c(\hat{\mathbf{k}}_3)c(-\hat{\mathbf{k}}_1-\hat{\mathbf{k}}_2-\hat{\mathbf{k}}_3)\right]. \quad (20)$$

The functions Γ are calculated from the two and higher order correlation functions of the monomer positions $\{\mathbf{r}^\alpha\}$ [2, 37, 39]. The free-energy in Eq. (20) can be decomposed as $F = F_0 + F_1 + \bar{F}$, where F_0, F_1 and $\bar{F}$ contain contributions from the zeroth replica sector, one replica sector and two or higher replica sector of $\psi(\hat{\mathbf{k}})$ and $c(\hat{\mathbf{k}})$, respectively. The cross-links couple different replica systems which manifests in a non-zero $\bar{F}$. In cross-linked homopolymers the system goes into a 'gel' or 'amorphous solid' state [33, 40] beyond a critical density of cross-links which is marked by the presence of a non-zero part in the higher replica sector of $c(\hat{\mathbf{k}})$ and a non-zero $\bar{F}$. In un-crosslinked di-block copolymer melts the system undergoes a first order microphase segregation transition for $f < 1/2$ [2] and a second order transition at $f = 1/2$ [41] from a disordered state to various ordered phases as the temperature is lowered below the transition temperature T_{ODT}.

B. Mean field phase diagram

We follow a variational calculation within a mean field approximation to study the equilibrium phases of the cross-linked copolymer system. The variational ansatz used for the density field $c(\hat{\mathbf{k}})$ is the same as the one proposed in Ref. [40] for homopolymers :

$$c(\hat{\mathbf{k}}) = c_M(\hat{\mathbf{k}}) = m[(1-q)\,\delta_{\hat{\mathbf{k}},\mathbf{0}} + q\,\delta_{\mathbf{k}_S,\mathbf{0}}\exp(-\xi^2 k^2)]\,, \quad (21)$$

where $\mathbf{k}_S = \sum_{\alpha=0}^{n}\mathbf{k}^\alpha$ and $k^2 = \hat{\mathbf{k}}\cdot\hat{\mathbf{k}} = \sum_{\alpha=0}^{n}\mathbf{k}^\alpha\cdot\mathbf{k}^\alpha$. The above ansatz describes a state where a fraction q of total number of monomers is localized in a region of size ξ. In uncrosslinked systems $\xi = \infty$. The cross-links couple the replicas as can be seen from the

partition function $\mathcal{Z}_{n+1}$ (Eq. 9) which can result in a finite ξ indicating the presence of a gel phase where fraction q of the total monomers is localized in a region of length scale ξ. The one replica sector part of $c_M(\hat{\mathbf{k}})$ is $c_M^\alpha(\mathbf{k}^\alpha) = m\,\delta_{\mathbf{k}^\alpha,0}$ implying that each replica system is incompressible. We perform a mean-field analysis of the free energy in the following way. We substitute $\bar{c}_M(\hat{\mathbf{k}})$ in the free-energy $\bar{F}$ and minimize $\bar{F}$ with respect to $\bar{c}_M(\hat{\mathbf{k}})$. $\bar{\psi}_M(\hat{\mathbf{k}})$ calculated from the condition $\delta\bar{F}/\delta\bar{\psi}_M(\hat{\mathbf{k}}) = 0$ is given to the lowest order in q as

$$\bar{\psi}_M(\hat{\mathbf{k}}) \;=\; -mq\,\frac{\Gamma_{c\psi}(\hat{\mathbf{k}})}{\Gamma_{\psi\psi}(\hat{\mathbf{k}})}\delta_{\mathbf{k}_S,\mathbf{0}}\exp(-\xi^2k^2)\left(1-\sum_{\alpha=0}^{n}\prod_{\beta=0,\beta\neq\alpha}^{n}\delta_{\mathbf{k}^\beta,0}\right)(1-\delta_{\hat{\mathbf{k}},0}) \qquad (22)$$

In the liquid state $\xi = \infty$ which imply both $\bar{c}_M = 0$ and $\bar{\psi}_M = 0$. In the gel state, where $1/\xi$ is small but non-zero both $\bar{c}_M$ and $\bar{\psi}_M$ do not vanish at large length scales ; *i.e.* $k \leq 1/\xi \to 0$ where $\bar{c}_M \to const$ and $\bar{\psi}_M \to (1-2f-f\mu^2)f(1-f)Nl_0^2k^2 + O(k^4)$ (see Appendix B). This would suggest that the effect of cross-linking is not significant at length scales much smaller than the localization length ξ. This fact is reflected in the change in T_{ODT} which will be discussed at the end of this section. The minimum of $\bar{F}[\bar{c},\bar{\psi}]$ is sought from the conditions $\partial\bar{F}[\bar{c},\bar{\psi}]/\partial q|_{q_m,\xi_m} = 0$ and $\partial\bar{F}[\bar{c},\bar{\psi}]/\partial\xi|_{q_m,\xi_m} = 0$. $\bar{F}[\bar{c}_M,\bar{\psi}_M]$ as shown in Appendix B is given by [42],

$$\begin{aligned}\beta\bar{F} &= -m\ln(\xi^2V^{-2/3})\left[\frac{3q^2}{2}\left(\frac{1}{2}-\frac{f^2\mu^2}{2}+a_2(f)\right)+a_3(f)q^3+O(q^4)\right]\\ &+\frac{mNl_0^2}{\xi^2}\left[\frac{3q^2}{4}b_2(f)+b_3(f)q^3+O(q^4)\right]+O(\xi^{-4}) \qquad (23)\end{aligned}$$

In the limit where $\xi \to \infty$ the term proportional to $\ln(\xi^2)$ is much larger than the term proportional to $1/\xi^2$ term, therefore we can minimize the coefficient of $\ln(\xi^2)$ with respect to q. Minimization obtains $q_m\,(-\epsilon + a_3(f)q_m) = 0$, where $\epsilon = f^2\mu^2/2 - 1/2 - a_2(f) = N_c - N_c^*$; $N_c = f^2\mu^2/2$ being the number of cross-links per chain and the critical cross-link per chain $N_c^* = 1/2 + a_2(f) = 1/2$ [43] (since $a_2(f) = 0$, see Appendix B). The solution $q_m = 0$ becomes unstable as $f^2\mu^2 > 1$ or $N_c > N_c^*$ and $q_m = \epsilon/a_3(f) + O(\epsilon^2)$. Minimizing $\bar{F}$ with respect to ξ^2 yields two solutions, *i.e.*, $1/\xi_m^2 = 0$ and $1/\xi_m^2 = \epsilon/(Nl_0^2b_2(f))$. The solution with finite ξ_m^2 becomes stable when $\epsilon > 0$ which can be seen by calculating $\partial^2\bar{F}/\partial\xi^2$. Next we compute $F_1[c_M^\alpha,\psi^\alpha]$ by substituting q_m and ξ_m. The free-energy $F_1[c_M^\alpha,\psi^\alpha]$ in the limit $n \to 0$ characterizes the order to disorder transition. $F_1[c_M^\alpha,\psi^\alpha]$ is given by (see Appendix B),

$$\beta F_1[c_M^\alpha,\psi^\alpha] = \sum_{\alpha=0}^{n}\Bigg[\int_{\mathbf{k}^\alpha}\left(\Gamma_{\psi\psi}(\mathbf{k}^\alpha)-\chi_{cr}-vN^2\chi^\alpha+A_2(\mathbf{k}^\alpha)\right)\psi^\alpha(\mathbf{k}^\alpha)\psi^\alpha(-\mathbf{k}^\alpha)+$$
$$\int_{\mathbf{k}_1^\alpha,\mathbf{k}_2^\alpha}\left(\Gamma^{(3)}_{\psi\psi\psi}(\mathbf{k}_1^\alpha,\mathbf{k}_2^\alpha)+A_3(\mathbf{k}^\alpha)\right)\psi^\alpha(\mathbf{k}_1^\alpha)\psi^\alpha(\mathbf{k}_2^\alpha)\psi^\alpha(-\mathbf{k}_1^\alpha-\mathbf{k}_2^\alpha)$$
$$+\int_{\mathbf{k}_1^\alpha,\mathbf{k}_2^\alpha,\mathbf{k}_3^\alpha}\Gamma^{(4)}_{\psi\psi\psi\psi}(\mathbf{k}_1^\alpha,\mathbf{k}_2^\alpha,\mathbf{k}_3^\alpha)\;\psi^\alpha(\mathbf{k}_1^\alpha)\psi^\alpha(\mathbf{k}_2^\alpha)\psi^\alpha(\mathbf{k}_3^\alpha)\psi^\alpha(-\mathbf{k}_1^\alpha-\mathbf{k}_2^\alpha-\mathbf{k}_3^\alpha)\Bigg]\,, \tag{24}$$

where

$$A_2(\mathbf{k}^\alpha) \;=\; \frac{1}{V}\Bigg(\int d\hat{\mathbf{k}}'\;\Gamma^{(4)}_{\psi\psi cc}(\mathbf{k}^\alpha,\hat{\mathbf{k}}',-\hat{\mathbf{k}}')\bar{c}_M(\hat{\mathbf{k}}')\bar{c}_M(-\hat{\mathbf{k}}')+\Gamma^{(4)}_{\psi\psi\psi\psi}(\mathbf{k}^\alpha,\hat{\mathbf{k}}',-\hat{\mathbf{k}}')\bar{\psi}_M(\hat{\mathbf{k}}')\bar{\psi}_M(-\hat{\mathbf{k}}')\Bigg) \tag{25}$$

and

$$A_3(\mathbf{k}^\alpha)=\frac{m}{V}\Gamma^{(4)}_{\psi\psi c}(\mathbf{0},\mathbf{k}_1^\alpha,\mathbf{k}_2^\alpha)\,. \tag{26}$$

In the above equation $\chi_{cr}=\mu^2V/(2m)$ and A_2 and A_3 can be calculated by substituting the ansatz for $\bar{c}_M$ (Eq. (21)) and $\bar{\psi}_M$ (Eq. (22)). In the disordered phase $\psi^\alpha=0$. Below the transition temperature T^{cr}_{ODT} ordering takes place on the length scale of $k_m^{-1}\propto N^{1/2}l_0$ where $\Gamma^{(2)}_{\psi\psi}(\mathbf{k})$ has a pronounced minimum. The different ordered states can be investigated from the ansatz [2] $\psi^\alpha(\mathbf{k}^\alpha)=1/\sqrt{l}\psi_l\sum_{i=1}^{l}[\delta(\mathbf{k}^\alpha+\mathbf{Q}_i)+\delta(\mathbf{k}^\alpha-\mathbf{Q}_i)]$, where $|\mathbf{Q}_i|\propto k_m$. T^{cr}_{ODT} can be calculated from the conditions $\partial F_1[\psi_l]/\partial\psi_l|_{\psi_l=\psi_l^*}=0$, $\partial^2F_1[\psi_l]/\partial\psi_l^2|_{\psi_l=\psi_l^*}>0$ and $F_1[\psi_l^*]=0$ at the disorder to order transition. The transition temperature T^{cr}_{ODT} is related to the transition temperature T_{ODT} of the uncrosslinked system as

$$T^{cr}_{ODT}=T_{ODT}\left(1+\frac{\bar{A}_2-N_cf^{-2}}{Nb}T_{ODT}\right)^{-1}\,, \tag{27}$$

where $\bar{A}_2=mV^{-1}A_2$. For cross-link densities $N_c<1$, $A_2=0$ and the transition temperature increases (Fig. 1) with the cross-link density as

$$T^{cr}_{ODT}=T_{ODT}(1-N_cf^{-2}T_{ODT}/Nb)^{-1}. \tag{28}$$

This basically reflects the fact that in the liquid state cross-links help ordering by bringing the B blocks together. However, when $N_c\geq N_c^*$ the system transforms into the gel state where $A_2>0$ (detailed calculations shown in Appendix C). $\bar{A}_2$ can be expressed as a function of the gel fraction q and the localization length ξ as

$$\bar{A}_2=q^2(t_0\ln(\xi^2)+t_1Nl_0^2/\xi^2+O(\xi^{-4}))+O(q^4)\,, \tag{29}$$

where t_0 and t_1 are positive constants. Both q and ξ^{-1} increase as the cross-link density increases which, in turn decreases T_{ODT}^{cr}. The system can be in different phases (as shown in Fig. 1) depending on the values of χN and N_c. The line $(\chi N)_t$ separates the disordered phases from the ordered phases. If $\chi N < (\chi N)_t$ the system undergoes a continuous transition from the liquid phase to the amorphous phase as N_c increases above N_c^*. A similar transition is also predicted for cross-linked homopolymers [33]. For cross-link densities $N_c < N_c^*$ the copolymer melt shows standard first order phase transition for $f < 1/2$ and a second order transition [41] at $f = 1/2$ [2, 37] from the disordered liquid phase to the ordered phase (lamellar phase) as the χN is increased above $(\chi N)_t$. In this regime, the cross-links increase the transition temperature slightly ; *i.e.*, $T_{ODT}^{cr} > T_{ODT}$ because the cross-links in the B blocks help phase segregation in the liquid state by bringing the B blocks together. The ordered phase at $\chi N > (\chi N)_t$ which can be viewed as an ordered phase in a liquid matrix (denoted as ordered phase I in Fig. 1) undergoes a continuous transition to an ordered phase in a gel matrix (denoted as ordered phase II in Fig. 1) as the cross-link density rises above N_c^*. This phase (ordered phase II) is different from the ordered phase in a liquid matrix (ordered phase I) in the following manner. In ordered phase II, a fraction q of the monomers is localized in a region of size ξ which is much larger than the radius of gyration $R_G \sim N^{1/2} l_0$. Since the ordering in the ψ field takes place on a length scale of the order of R_G we observe ordered structures within the region ξ. However ξ decreases as N_c increases and the ordered structures cease to exist when $\xi < R_G$. Thus the ordered solid transforms into the disordered solid as N_c is increased. The point B is a bi-critical point [45] where both the critical lines for liquid to disordered solid and ordered liquid to ordered solid meet.

III. EXPERIMENTAL METHODS

A polystyrene-polyisoprene (SI) copolymer was synthesized and characterized by methods described in ref. [31]. The weight-averaged molecular weights of the polystyrene and polyisoprene blocks were 8×10^3 g/mol and 24×10^3 g/mol, respectively, and we refer to the polymer as SI(8-24). The volume fraction of polystyrene, f, was determined to be 0.210, using NMR spectroscopy. The ratio of the weight to number averaged molecular weights (M_w/M_n) was estimated by gel permeation chromatography to be 1.03. The glass transition temperature (T_g) of the polystyrene microphase was determined, using a TA Instruments

DSC model 2920 with a heating rate of 10°C/min, to be 51°C.

Mixtures of dicumyl peroxide (DCP) and SI(8-24) were prepared by dissolving predetermined amounts of the components in benzene. The mixture was dried first at room temperature for 20 h, followed by further drying in a vacuum oven at 70°C for 4 h. The final DCP concentration in the mixture was determined by weighing the dry mixture. The finite vapor pressure of DCP at 70°C led to measurable losses of DCP during sample preparation.

DCP/SI(8-24) mixtures were molded into disks with 10 mm diameter and 1 mm thickness using a Carver press at room temperature. The disk was placed in a Parr high-pressure vessel and heated for 2 hrs at 160°C and 300 psi under a nitrogen blanket. This led to the formation of bubble-free cross-linked samples. All of the experiments described below were performed on the disks thus obtained. Samples are labeled according to the weight % of DCP which ranged from 0.40 to 4.06 % (Table 1). Reheating the samples to 160°C resulted in no changes in the properties of the sample as measured by the probes given below. We thus conclude that our synthesis protocol leads to complete consumption of the cross-linking reagent. We also subjected disks of homopolystyrene and homopolyisoprene to the same protocol and found that the homopolystyrene molecular weight remained unchanged, while the homopolyisoprene was converted to a cross-linked gel. It is thus obvious that our protocol results in the selective cross-linking of the polyisoprene chains.

The network structure of our samples was studied by immersing them in toluene, a good solvent for both polystyrene and polyisoprene, while order-disorder transition temperatures were determined by birefringence and SAXS. Birefringence experiments were conducted on an apparatus described in ref. [46]. The samples were capped with fused quartz windows, placed in a thermostated oven between crossed polarizers, and the fraction of incident light power (from a *Nd*: YAG laser with wavelength $\lambda = 532$ nm) that was transmitted (I/I_0) was monitored as a function of thermal history. SAXS experiments were performed on beam line 1-4 of the Stanford Synchrotron Radiation Laboratory (SSRL) using samples encased between Kapton windows. The following is the configuration of the beamline: X-ray wavelength $\lambda = 1.488\,\text{Å}$, wavelength spread $\sim 1\%$, and beam diameter ~ 0.5 mm. The reciprocal space, ranging from $k = 0.076$ nm^{-1} to 1.6 nm^{-1} (where, $k = 4\pi \sin(\theta/2)/\lambda$), was probed for this measurement. The samples were held between Kapton films inside a thermostated oven. The scattering pattern was recorded with a CCD camera and azimuthally averaged. After the subtraction of the background and empty cell scattering, the measured scattering

data were converted to absolute scattering intensity using a secondary standard provided by SSRL.

IV. EXPERIMENTAL RESULTS

Cross-linked samples weighing about 0.02 g were immersed in excess toluene for 12 h. Samples with DCP wt. % $\leq$ 0.6 dissolved completely, leaving no trace of a gel. These samples also did not maintain their shape when heated in the dry state to 160°C. Immersing samples with DCP wt. % $\geq$ 0.65% in excess toluene resulted in the formation of a swollen gel. These samples also maintained their shape when heated in the dry state to 160°C. We conclude that the gel point of our cross-linked samples is obtained when the DCP wt. % is in the vicinity of 0.65. The polymer volume fraction in the swollen state ϕ was determined by weighing the swollen gels. We accounted for the difference in densities of toluene and SI(8-24), but ignored the volume change of mixing. The values of ϕ thus obtained are given in Table 1.

According to the Flory-Erman theory (FE) [13] homopolymer networks undergoing affine deformation during swelling, ϕ obeys the relationship

$$\ln(1-\phi)+\chi\phi^2+\phi=-\left(\frac{X}{V_0}\right)V_1\phi^{1/3}\left[1+\frac{\mu}{X}(1-\phi^{-2/3})\right] \tag{30}$$

where χ is the Flory-Huggins interaction parameter between monomers of the polymer chain and the solvent, V_0 is the unswollen sample volume, and V_1 is the molar volume of solvent. Parameters X and μ depend on the network structure. For randomly cross-linked networks Mark and coworkers have shown that [47, 48]

$$\frac{X}{V_0}=\frac{\rho(N_c-3)}{2M_n} \tag{31}$$

$$\frac{\mu}{V_0}=\frac{\rho(N_c-1)}{2M_n} \tag{32}$$

where ρ is the polymer density, M_n is the number-average molecular weight of the polymer precursor and N_c is the average number of cross-links per chain.

Eqs. 30-32 are strictly applicable to randomly cross-linked homopolymers. Our system is considerably more complex because we have randomly cross-linked one of the blocks of

a block copolymer. Unfortunately, theories that address the swelling of cross-linked block copolymers have not yet been developed. Lacking a better alternative, we used Eqs 30-32 to obtain an estimate of N_c, with the measured values of ϕ and $M_n = 32$ kg/mol. Due to the absence of a measured χ between the cross-linked SI block copolymers and toluene, we used $\chi = 0.371$, a volume averaged value of $\chi_{ps} = 0.41$ (polystyrene and toluene) and $\chi_{pi} = 0.36$ (polyisoprene and toluene) [49]. The values of N_c thus obtained are denoted as N_c^{FE} and given in Table 1. Extensive characterization of polyisoprene networks obtained by DCP cross-linking has led to the conclusion that one cross-link per DCP molecule is obtained in the system [50]. We can thus obtain a second estimate of N_c from the DCP concentration in our samples. This estimate is called N_c and is also given in Table 1. It is clear from Table 1 that there is reasonable consistency between N_c and N_c^{FE}. Due to the many unanswered questions regarding the applicability of the FE theory to cross-linked block copolymers, we have chosen to use N_c as a measure of the cross-linking density of our samples.

In Figure 2, we show typical small angle X-ray scattering profiles, $I(k)$, obtained from our samples. We restrict attention to temperatures between 70°C (above T_g) and 170°C (just above the cross-linking temperature). The data were obtained as a function of increasing temperature with 10 min equilibration time at each temperature. At 70°C, $I(k)$ from the pure block copolymer, SI[0.00], contains a primary peak at $k_m = 0.31$ nm^{-1}, a second order peak at $k_2 = 0.53$ nm^{-1} (Figure 2a). The ratio k_2/k_m is about $\sqrt{3}$ which is in agreement with that expected from cylinders arranged on a hexagonal lattice [51, 52]. The scattering profiles of SI[0.00] are sensitive functions of temperature. The primary peak scattering intensity $I(k_m)$ changes by a factor of 10 in our temperature window. The qualitative characteristics of $I(k)$ change abruptly when T is increased from 100 to 110°C: the width of the primary peak increases abruptly and the second order peak vanishes. This is a standard signature of an order-to-disorder transition [53, 54, 55, 56]. We thus conclude that T_{ODT} of SI[0.00] is 105 ± 5°C.

In Figures 2b, 2c, 2d, and 2e we show $I(k)$ measured from SI[0.65], SI[1.16], SI[1.94], and SI[4.06], respectively. We see that cross-linking suppresses the second order scattering peak [compare Figs. 2(a) and 2(b), for example]. The primary scattering peak is thus the dominant feature of the SAXS profiles from our cross-linked solids. The scattering peak at high temperatures (above 110°C) from SI[0.00] - Figure 2(a) - is due to concentration fluctuations. The SAXS profiles in Figures 2(a) through 2(d) at 170°C are independent of

DCP concentration (see Figures 2a-d). This implies that cross-linking has little effect on the concentration fluctuations obtained in the disordered state when the DCP wt. % is less than 1.94. In contrast, the structure of the ordered phase is strongly affected by cross-linking, as can be seen by examining the scattering profiles at 70°C at various cross-linking densities (Figures 2(a) through 2(d)). At very high cross-linking density, we find that SAXS intensity at 170°C is suppressed. This can be seen by comparing the data obtained from SI[4.06] (Figure 2e) with that obtained from the samples with lower cross-linking density. This indicates very high cross-linking densities can lead to homogenization of our sample. Since we are primarily interested in solid samples that undergo reversible order-disorder transitions, the remainder of the paper is focused on samples DCP wt. % ≤ 1.94.

The scattering profiles from ordered phases are often expressed as a product $P(k)S(k)$, where $S(k)$ is the contribution due to the periodicity and $P(k)$ is the form factor of the individual structures that are placed on the periodic lattice (e.g. cylinders). We propose a natural extension of this for periodic structures made up of chain molecules,

$$I(k) = P(k)S(k)C(k) \tag{33}$$

where $C(k)$ is the contribution due to chain connectivity. $C(k)$ will become irrelevant in the strong segregation limit (i.e. $C(k) \to 1$) where mixing between the two blocks is not permitted except in the infinitely thin interface between the microphases. It is clear, however, that our systems are far from the strong segregation limit [2, 57, 58, 59]. In the disordered state, when $T \gg T_{ODT}$, $I(k)$ is dominated by chain connectivity contributions. We thus used the measured scattering profile at the highest temperature 170°C, $I(k)_{T=170^\circ C}$ as a measure of $C(k)$ and define a normalized scattering intensity

$$I_N(k) = I(k)/I(k)_{T=170^\circ C}\,. \tag{34}$$

It should be clear from the arguments given above that $I_N(k)$ will be dominated by the form factor $P(k)$ and the structure factor $S(k)$. Typical results for $I_N(k)$ are shown in Figure 3a.where we show results obtained from SI[0.70] at 70°C. The arrows represent the locations of $\sqrt{3}k_m$, and $\sqrt{7}k_m$ expected from a hexagonal lattice [60]. Plots of the normalized intensity show clear evidence of the higher order peaks corresponding to a hexagonal phase (Figure 3a). In contrast, the $I(k)$ profiles shown in the inset of Figure 3a show virtually no evidence of higher order peaks.

In order to estimate the area under the higher order peaks, we approximate the scattering profile in the region $0.4 < k < 1.6$ by the functional form

$$I(k) = b_1 \exp\left(-\frac{(k-b_2)^2}{b_3}\right) + c_1 \exp\left(-\frac{(k-c_2)^2}{c_3}\right) + \left(a_1 + \frac{a_2}{k-a_3}\right) \tag{35}$$

where, $a_1, a_2, a_3, b_1, b_2, b_3, c_1, c_2$, and c_3 are fitting parameters. The first two terms in Eq. 35 account for the $\sqrt{3}k_m$, and $\sqrt{7}k_m$ peaks while the last term accounts for the $q-$dependence of the background. The curve in Figure 3a is the least squares fit of Equation 35 through the data. The fitting procedure enables determination of the area under the second order peak $A_2 = b_1\sqrt{\pi b_3}$.

Figures 3b-d show the effect of increasing temperature on $I_N(k)$ for SI[0.70]. It is evident that the higher order peaks diminish in intensity with increasing temperature. At 150°C we see the higher order peaks are no longer evident [Figure 3(d)]. The solid curves in Figures 3b-d are least-squares fits to Equation 35, and they enable determination of the temperature dependence of A_2 for SI[0.70].

We obtained $I_N(k)$ from all of the samples listed in Table 1, and estimated the temperature dependence of A_2 using Equation 35 as described above. The results are shown in Figure 4a were A_2 from different samples is plotted as a function of temperature. The finite values of A_2 obtained at temperatures ≤ 110°C from samples with DCP wt. % ≤ 1.06 clearly indicate the presence of a hexagonal ordered phase in this temperature range. Since A_2 is related to the extent of long-range order in our system, which, in turn, must depend on cross-linking density, it is no surprise that the values of A_2 depend on cross-linking density. We expect a decrease in long-range order with increasing cross-linking density. This is consistent with the trends seen in Figure 4a. A point worth noting, however, is that values of A_2 from samples with DCP wt. % ≤ 1.06 at a given temperature are comparable in magnitude. For example, A_2 at 70°C from the pure block copolymer SI[0.00] is 0.058 while that from SI[1.06] at the same temperature is 0.038. This implies that the intensity of the second order peak in both uncrosslinked and cross-linked samples is similar. This is not at all obvious in the unnormalized $I(k)$ data shown in Figure 2 (compare Figure 2a and 2c). Recall that our samples were made by cross-linking the disordered state at 160°C. It is clear that when the DCP wt. % ≤ 1.06 the ordered phase reappears upon cooling.

An abrupt change in ordering behavior is seen in Figure 4a when the DCP wt. % is increased from 1.06 to 1.16. For samples with DCP wt. % is ≥ 1.16 we see negligible values

of A_2 across the entire temperature window. This implies that when the DCP wt. % is ≥ 1.06 the ordered phase does not reappear upon cooling.

It is clear from Figure 4a that at temperatures $\geq 120°$C the values of A_2 for all our samples reaches a "baseline" that lies between 0.01 and 0.00. Deviations from this baseline were considered as signatures of an ordered phase. Our method for determining T_{ODT} from the SAXS data is shown in Fig. 4b where we show the temperature dependence of A_2 of SI[0.70]. We fit a straight line through the high temperature data ($T \geq 130°$C) and identified the first point of departure from this line as the order-disorder transition. We identified T_{ODT} of all of the samples with DCP wt. % $\leq .06$ in this manner.

Birefringence measurements can also be used to detect the presence of anisotropic structures such as lamellar and hexagonal phases in block copolymers [31, 62]. Figure 5 shows the temperature dependence of light intensity I leaking through our samples held between crossed polarizers, normalized by the incident intensity (I_0). We find that the temperature dependence of I/I_0, shown in Figure 5, is similar to that of A_2, shown in Figure 4. Samples with DCP wt. % ≤ 1.06 show finite birefringence signals at low temperatures. In contrast, samples with DCP wt. % ≥ 1.16 show negligible birefringence at all accessible temperatures. The birefringence signal I/I_0 from samples with DCP wt. % ≤ 1.06 approach "baseline" values ranging from 0.03-0.00. We estimate T_{ODT} from the birefringence data using the same methodology as that described above for the SAXS data (see Figure 4b). The birefringence data confirm all of the conclusions made on the basis of the SAXS data.

We are interested in solids that undergo reversible order-disorder transitions. In Figure 6(a) we show the temperature dependence of the SAXS peak intensity I_m obtained from SI[0.70] during a heating and cooling cycle. It is clear that the changes in the sample structure as seen in the SAXS data are reversible. In addition there is no evidence of hysteresis in the data shown in Fig. 6a. In Figure 6(b) we show the birefringence results obtained in heating and cooling cycles from samples SI[0.70]. It is evident that SI[0.07] must be supercooled substantially below T_{ODT} before the signatures of a fully ordered sample are obtained. The absence of hysteresis in the SAXS measurements and the presence of hysteresis in the birefringence measurements was observed in all of the samples with DCP wt. % ≤ 1.06. This is due to the difference in length scales probed by the two techniques. SAXS probes the local structure on the length scale of the periodicity of the ordered phase (20 nm) while the birefringence measurements probe the structure on the length scales of the

ordered grains (1 μm). The data shown in Figure 6(b) were obtained from two independent heating and cooling cycles. There is virtually no difference between the birefringence data obtained from the two cycles. It is thus clear that the order-disorder transitions in our solids can be accessed repeatedly and reversibly. We have thus accomplished our objective as stated in the Introduction.

V. DISCUSSION

In Figure 7, we show the dependence of T_{ODT} on cross-linking density as measured by both birefringence measurements and SAXS. We use a dimensionless parameter $N_{c,\,norm} = N_c/(N_c$ at gelation point) to quantify the cross-linking density (abscissa in Figure 7). The solid lines in Figure 7 represent the experimentally determined phase diagram. The phase diagram contains three kinds of phases: disordered liquids (DL), disordered solids (DS), and ordered solids (OS). The ordered solid is confined to a region of box-like shape indicating the presence of two regimes: (1) a regime where T_{ODT} is independent of temperature ($N_{c,\,norm}$ when ≤ 1.7) and (2) a regime where ordered solids cannot be observed in our experimental window ($N_{c,\,norm} > 1.7$).

The dashed curve in Figure 7 represents the theoretically predicted boundary of the ordered solid phase (OS). The temperature dependence of the Flory-Huggins interaction parameter χ between polystyrene and polyisoprene is known ($\chi = 0.0064{+}20.0/T$ [31]). This enables a direct comparison between theory and experiment with no adjustable parameters. For the theoretical curve, $N_{c,\,norm} = 2N_c$ because N_c at the gel point is 0.5 (Figure 1). The dashed curve in Fig. 7 is obtained by with these inputs and the results given in Fig. 1. It is evident in Fig. 7 that the theoretical phase diagram captures the essential features of the experimental observations: namely the existence of two regimes. There are however, two differences between theory and experiment. (1) The theory predicts that T_{ODT} increases from 115°C to 130°C with cross-linking density when $N_{c,\,norm}$ is less than unity. The experimental data does not support this conclusion. While the scatter in the data do not rule out an increase in T_{ODT} with increasing cross-linking density, the magnitude of the increases, if is exists, is some what smaller than that predicted theoretically. (2) The value of N_c at the gel point in theory is 0.5 (Figure 1) while that obtained experimentally is 1.49 (Table 1). These discrepancies reflect the complexity of cross-linked systems. It is

worth noting that many aspects of cross-linked homopolymer systems are not completely understood [63, 64].

To our knowledge, the fact that block copolymer chains composed of hundreds of repeat units can undergo reversible order-disorder transitions despite the attachment of one of the blocks to a cross-linked network has not been shown in previous studies [15, 16, 17, 18, 19, 20, 21, 22, 23, 24, 25]. However liquid crystalline elastomers [7, 65, 66, 67], wherein low molar mass mesogens covalently attached to an elastomeric network, do exhibit reversible nematic-to-isotropic phase transitions in response to changes in temperature. Considerable insight into the phase behavior of these systems has been obtained through a combination of careful synthesis, characterization, and theory [7, 65]. In a closely related study Sakurai et al. [23] examined the effect of cross-linking on the morphology of a polystyrene-block-polybutadiene-block-polystyrene (SBS) copolymer. The SBS copolymer exhibited a lamellar phase in bulk at all accessible temperatures. A disordered sample was prepared by adding adequate amounts of dioctylphthalate (DOP), a common solvent for the both polystyrene and polybutadiene blocks. The polybutadiene blocks were cross-linked in the disordered state and the DOP was then solvent-extracted to obtain a dry but cross-linked SBS sample. It was found that these cross-linked SBS samples were disordered. However, annealing these samples led to the reappearance of the lamellar phase. This study demonstrates that cross-linking does not impede order formation when the driving forces for order formation are sufficiently large. The changes in structure seen in the cross-linked SBS samples upon annealing are, however, irreversible. There was no possibility of obtaining a disordered phase in these cross-linked samples because the order-disorder transition of the block copolymer was inaccessible even in the absence of cross-links. The materials studied in ref. [23] were thus not suitable for studying reversible order-disorder transitions in cross-linked block copolymers.

VI. CONCLUSIONS

We have accomplished our goal of synthesizing and characterizing cross-linked block copolymer solids that undergo reversible order-disorder transitions, thereby opening the door to applications such as shape memory materials and artificial muscles. Ordered solids were synthesized by selectively cross-linking the polyisoprene chains of a polystyrene-polyisoprene

block copolymer, at temperatures well above

the order-disorder transition of the pure block copolymer in the absence of cross-links. The resulting networks were characterized by swelling experiments, which gave N_c, the average number of cross-links per chain, and birefringence and SAXS experiments which enabled the determination of the order-disorder transition temperature, T_{ODT}, as a function of N_c. Two regimes of behavior were observed: (1) below a critical value of N_c, T_{ODT} was a weak function of cross-linking density, and (2) above a critical value of N_c, T_{ODT} decreases extremely rapidly with cross-linking density. We also developed a field theoretic model to understand the origin of this behavior. Below a critical cross-link density $N_c^* = 0.5$ the system undergoes the standard microphase segregation transformation as the temperature is lowered below the transition temperature T_{ODT}. For cross-link densities above the critical cross-link density the monomers are localized within a region of size $\xi \sim (N_c - N_c^*)^{-1/2}$. If the localization length is much larger than the radius of gyration (i.e $\xi \gg R_g$) the chains microphase separate within that length scale giving rise to a different ordered phase (ordered phase II) compared to the ordered phase of the uncrosslinked chains (ordered phase I). The ordering transition cease to exist as ξ becomes comparable to R_g which is reflected in the sharp decrease of T_{ODT} for $N_c > N_c^*$. The theory thus provides the microscopic underpinnings of the unusual phase behavior obtained from our cross-linked block copolymer samples.

Acknowledgments

We thank Jatin U. Mody for conducting the first experiments on cross-linked block copolymers, and Jian Liu for helpful discussions. We gratefully acknowledge the financial support, provided by the National Science Foundation (DECS 0103297) and the Department of Energy (Materials Sciences Division of Lawerence Berkeley National Lab). This work was supported by Department of Energy Contract No. DE-AC03-76SF00515.

APPENDIX A: DERIVATION OF THE FREE ENERGY FUNCTIONAL WITHIN RPA

In this appendix we set out to derive the partition function $\mathcal{Z}_{n+1}$ in terms of the density variables $\rho_A(\hat{\mathbf{r}})$ and $\rho_B(\hat{\mathbf{r}})$ using the Random Phase Approximation (RPA). The partition function $\mathcal{Z}_{n+1}$ is defined as,

$$\begin{aligned}
\mathcal{Z}_{n+1} &= \int \mathcal{D}[\rho_A(\hat{\mathbf{r}})]\mathcal{D}[\rho_B(\hat{\mathbf{r}})]\delta\left(\rho_A(\hat{\mathbf{r}}) - \sum_{i=1}^{m}\int_0^f ds \prod_{\alpha=0}^{n}\delta(\mathbf{r}^\alpha - \mathbf{r}_i^\alpha(s))\right) \\
&\quad \times\delta\left(\rho_B(\hat{\mathbf{r}}) - \sum_{i=1}^{m}\int_f^1 ds \prod_{\alpha=0}^{n}\delta(\mathbf{r}^\alpha - \mathbf{r}_i^\alpha(s))\right) \\
&\quad \times \int \mathcal{D}[\mathbf{r}_i^\alpha(s)]\exp\left[-\sum_{\alpha=0}^{n}\left\{\sum_{i=1}^{m}\frac{3}{2Nl_0^2}\int_0^1 ds\left(\frac{d\mathbf{r}_i^\alpha}{ds}\right)^2 + V(\{\mathbf{r}_i^\alpha\})\right\} + \frac{\mu^2}{2m}\int d\hat{\mathbf{r}}\ \rho_B(\hat{\mathbf{r}})\rho_B(\hat{\mathbf{r}})\right] \\
&= \int \mathcal{D}[\rho_A(\hat{\mathbf{r}})]\mathcal{D}[\rho_B(\hat{\mathbf{r}})]\mathcal{D}[\gamma_A(\hat{\mathbf{r}})]\mathcal{D}[\gamma_B(\hat{\mathbf{r}})]\Bigg\{\exp\left[i\int d\hat{\mathbf{r}}\left(\rho_A(\hat{\mathbf{r}})\gamma_A(\hat{\mathbf{r}}) + \rho_B(\hat{\mathbf{r}})\gamma_B(\hat{\mathbf{r}})\right)\right. \\
&\quad \left. + \frac{\mu^2}{2m}\int d\hat{\mathbf{r}}\ \rho_B(\hat{\mathbf{r}})\rho_B(\hat{\mathbf{r}}) - vN^2\sum_{\alpha=0}^{n}\chi^\alpha\int d\mathbf{r}^\alpha\left(\rho_A^\alpha(\mathbf{r}^\alpha)\rho_A^\alpha(\mathbf{r}^\alpha) + 2\rho_A^\alpha(\mathbf{r}^\alpha)\rho_B^\alpha(\mathbf{r}^\alpha) + \rho_B^\alpha(\mathbf{r}^\alpha)\rho_B^\alpha(\mathbf{r}^\alpha)\right)\right] \\
&\quad \times \int \mathcal{D}[\hat{\mathbf{r}}_i(s)]\, P_A(\{\hat{\mathbf{r}}_i\})P_B(\{\hat{\mathbf{r}}_i\})\Bigg\}
\end{aligned} \tag{A1}$$

where

$$P_A(\{\hat{\mathbf{r}}_i\}) = \exp\left[-\sum_{i=1}^{m}\int_0^f ds\left\{\frac{3}{2Nl_0^2}\left(\frac{d\hat{\mathbf{r}}_i}{ds}\right)^2 + i\gamma_A(\hat{\mathbf{r}}_i(s))\right\}\right] \tag{A2}$$

and

$$P_B(\{\hat{\mathbf{r}}_i\}) = \exp\left[-\sum_{i=1}^{m}\int_f^1 ds\left\{\frac{3}{2Nl_0^2}\left(\frac{d\hat{\mathbf{r}}_i}{ds}\right)^2 + i\gamma_B(\hat{\mathbf{r}}_i(s))\right\}\right]. \tag{A3}$$

One can expand $\langle Q\rangle = \int \mathcal{D}[\hat{\mathbf{r}}_i(s)]\, P_A(\{\hat{\mathbf{r}}_i\})P_B(\{\hat{\mathbf{r}}_i\})$ as a power series in $\gamma_{A,B}(\hat{\mathbf{r}})$ and write $\langle Q\rangle = \exp(\ln\langle Q\rangle)$. In order to evaluate $\mathcal{Z}_{n+1}$ we need to calculate the integrals in $\gamma_{A,B}(\hat{\mathbf{r}})$ which are approximated using RPA. According to RPA [27, 37] the integrand $\exp[i\int d\hat{\mathbf{r}}\,(\rho_A(\hat{\mathbf{r}})\gamma_A(\hat{\mathbf{r}}) + \rho_B(\hat{\mathbf{r}})\gamma_B(\hat{\mathbf{r}})) + \ln\langle Q\rangle] = \exp[F_\gamma[\gamma_A,\gamma_B,\rho_A,\rho_B]]$ is replaced by $\exp[F_\gamma[\gamma_A^*,\gamma_B^*,\rho_A,\rho_B]]$ where $\delta F_\gamma[\gamma_A,\gamma_B,\rho_A,\rho_B]/\delta\gamma_A\,|_{\gamma_A^*,\gamma_B^*} = 0$ and $\delta F_\gamma[\gamma_A,\gamma_B,\rho_A,\rho_B]/\delta\gamma_B\,|_{\gamma_A^*,\gamma_B^*} = 0$. The above conditions yield to linear order in ρ_A and

ρ_B,

$$\gamma_A = i(W_{11}\rho_A + W_{12}\rho_B)$$
$$\gamma_B = i(W_{21}\rho_A + W_{22}\rho_B) \tag{A4}$$

where in Fourier space, $W_{11} = Vm^{-1}f^2 g_2(fx)/D$, $W_{12} = -Vm^{-1}f(1-f)g_{12}(fx,(1-f)x)/D = W_{21}$ and $W_{22} = Vm^{-1}(1-f)^2 g_2((1-f)x)/D$, where $D = f^2(1-f)^2[g_2(fx)g_2((1-f)x) - g_{12}(fx,(1-f)x)^2]$. $g_2(y) = 2/y^2(y + \{\exp(-y) - 1\})$ is the Debye function [37]. $g_{12}(x,y) = 1/(xy)(1 + \exp(-x-y) - \exp(-x) - \exp(-y))$ and $x = Nl_0^2(\hat{\mathbf{k}}\cdot\hat{\mathbf{k}})/6$. Substituting $\rho_A = \psi + fc$ and $\rho_B = (1-f)c - \psi$ we get the free-energy F given by Eq. (20). It turns out

$$\Gamma^{(2)}_{\psi\psi} = \Gamma_{\psi\psi} - \chi_{cr} - vN^2 \sum_{\alpha=0}^{n} \chi^\alpha \prod_{\beta=0,\,\beta\neq\alpha}^{n} \delta_{\mathbf{k}^\beta,\mathbf{0}} \tag{A5}$$

where $\Gamma_{\psi\psi} = \frac{1}{2}(W_{11} + W_{22} - 2W_{12})$, $\chi_{cr} = \mu^2 V/2m$ and $\chi^\alpha = v^\alpha_{11}/2 + v^\alpha_{22}/2 - v^\alpha_{12}$. $\Gamma_{\psi\psi}$ can be approximated very well by the following form [37] which is based on the asymptotic forms of the function at $\hat{\mathbf{k}} \to 0$ and at $\hat{\mathbf{k}} \to \infty$.

$$\Gamma_{\psi\psi}(\hat{\mathbf{k}}) = \frac{Vm^{-1}}{2}\left(\frac{Nl_0^2k^2}{12f(1-f)} + \frac{9}{Nl_0^2f^2(1-f)^2k^2} - \frac{s(f)}{f(1-f)}\right) \tag{A6}$$

The function $s(f) \sim O(1)$ is introduced to keep the function within 4% accuracy [37]. Clearly $\Gamma_{\psi\psi}(\hat{\mathbf{k}})$ has a minimum at $k_m^2 = \sqrt{108/[f(1-f)N^2l_0^4]}$. The value of $\Gamma_{\psi\psi}(\hat{\mathbf{k}})$ at $k = k_m$ is

$$\Gamma_{\psi\psi}(k_m) = \frac{N}{2\rho_0}\left(\sqrt{\frac{3}{f^3(1-f)^3}} + \frac{s(f)}{f^2(1-f)^2}\right) = \frac{N}{2\rho_0}\chi_s \tag{A7}$$

$$\Gamma^{(2)}_{c\psi} = fW_{11} + (1-2f)W_{12} - (1-f)W_{22} - u_{cr} + N^2 \sum_{\alpha=0}^{n} u^\alpha \prod_{\beta=0,\,\beta\neq\alpha}^{n} \delta_{\mathbf{k}^\beta,\mathbf{0}} \tag{A8}$$

$$\Gamma^{(2)}_{cc} = \frac{1}{2}(f^2W_{11} + 2f(1-f)W_{12} + (1-f)^2W_{22}) - w_{cr} + N^2 \sum_{\alpha=0}^{n} w^\alpha \prod_{\beta=0,\,\beta\neq\alpha}^{n} \delta_{\mathbf{k}^\beta,\mathbf{0}} \tag{A9}$$

where $\rho_0 = V/(mN)$, $u^\alpha = fv^\alpha_{11} + (1-2f)v^\alpha_{12} - (1-f)v^\alpha_{22}$, $u_{cr} = f\mu^2 V/m$, $w^\alpha = \frac{1}{2}(f^2v^\alpha_{11} + 2f(1-f)v^\alpha_{12} + (1-f)^2v^\alpha_{22})$ and $w_{cr} = f^2\mu^2 V/2m$. The calculation of the terms higher than the quadratic order in ρ_A and ρ_B are straightforward but tedious. However we will need only the values of the functions in the $\hat{\mathbf{k}} \to 0$ limit which will be shown at appropriate places.

APPENDIX B: CALCULATION OF $\bar{F}$

1. Contribution from the many replica sector of c_M and ψ_M

We calculate the part ($\bar{F}$) of the free energy $F[\psi, c]$ which arises due to the many replica sector part of the density field $\bar{c}$ and the order parameter field $\bar{\psi}$. Since both $\bar{c}$ and $\bar{\psi}$ are proportional to q, $\bar{F}$ can be calculated as a polynomial in q and for a cross-link density close to N_c^*, q is small and terms in lower powers of q are more significant. The contribution to the term proportional to q^2 in $\bar{F}$ is from the following terms :

$$\int d\hat{\mathbf{k}} \left[\left(\Gamma^{(2)}_{cc}(\hat{\mathbf{k}}) + \frac{3m}{V} \Gamma^{(3)}_{ccc}(\mathbf{0}, \hat{\mathbf{k}}) + \frac{6m^2}{V^2} \Gamma^{(4)}_{cccc}(\mathbf{0}, \mathbf{0}, \hat{\mathbf{k}}) \right) \bar{c}_M(\hat{\mathbf{k}}) \bar{c}_M(-\hat{\mathbf{k}}) + \left(\Gamma^{(2)}_{\psi\psi}(\hat{\mathbf{k}}) + \frac{m}{V} \Gamma^{(3)}_{\psi\psi c}(\mathbf{0}, \hat{\mathbf{k}}) \right.$$
$$\left. + \frac{m^2}{V^2} \Gamma^{(4)}_{\psi\psi cc}(\mathbf{0}, \mathbf{0}, \hat{\mathbf{k}}) \right) \bar{\psi}_M(\hat{\mathbf{k}}) \bar{\psi}_M(-\hat{\mathbf{k}}) + \left(\Gamma^{(2)}_{\psi c}(\hat{\mathbf{k}}) + \frac{2m}{V} \Gamma^{(3)}_{\psi cc}(\mathbf{0}, \hat{\mathbf{k}}) + \frac{3m^2}{V^2} \Gamma^{(4)}_{\psi ccc}(\mathbf{0}, \mathbf{0}, \hat{\mathbf{k}}) \right)$$
$$\left. \times \bar{c}_M(\hat{\mathbf{k}}) \bar{\psi}_M(-\hat{\mathbf{k}}) \right] \tag{B1}$$

The part proportional to q^3 is from:

$$\int d\hat{\mathbf{k}}_1 d\hat{\mathbf{k}}_2 \left[\left(\Gamma^{(3)}_{ccc}(\hat{\mathbf{k}}_1, \hat{\mathbf{k}}_2) + \frac{4m}{V} \Gamma^{(4)}_{cccc}(\mathbf{0}, \hat{\mathbf{k}}_1, \hat{\mathbf{k}}_2) \right) \bar{c}_M(\hat{\mathbf{k}}_1) \bar{c}_M(\hat{\mathbf{k}}_2) \bar{c}_M(-\hat{\mathbf{k}}_1 - \hat{\mathbf{k}}_2) + \left(\Gamma^{(3)}_{\psi\psi\psi}(\hat{\mathbf{k}}_1, \hat{\mathbf{k}}_2) + \right.$$
$$\left. \frac{m}{V} \Gamma^{(4)}_{\psi\psi\psi c}(\mathbf{0}, \hat{\mathbf{k}}_1, \hat{\mathbf{k}}_2) \right) \bar{\psi}_M(\hat{\mathbf{k}}_1) \bar{\psi}_M(\hat{\mathbf{k}}_2) \bar{\psi}_M(-\hat{\mathbf{k}}_1 - \hat{\mathbf{k}}_2) + \left(\Gamma^{(3)}_{\psi\psi c}(\hat{\mathbf{k}}_1, \hat{\mathbf{k}}_2) + \frac{2m}{V} \Gamma^{(4)}_{\psi\psi cc}(\mathbf{0}, \hat{\mathbf{k}}_1, \hat{\mathbf{k}}_2) \right)$$
$$\left. \times \bar{\psi}_M(\hat{\mathbf{k}}_1) \bar{\psi}_M(\hat{\mathbf{k}}_2) \bar{c}_M(-\hat{\mathbf{k}}_1 - \hat{\mathbf{k}}_2) + \left(\Gamma^{(3)}_{\psi cc}(\hat{\mathbf{k}}_1, \hat{\mathbf{k}}_2) + \frac{3m}{V} \Gamma^{(4)}_{\psi ccc}(\mathbf{0}, \hat{\mathbf{k}}_1, \hat{\mathbf{k}}_2) \right) \bar{\psi}_M(\hat{\mathbf{k}}_1) \bar{c}_M(\hat{\mathbf{k}}_2) \bar{c}_M(-\hat{\mathbf{k}}_1 - \hat{\mathbf{k}}_2) \right] \tag{B2}$$

There will also be contributions to the q^3 term in $\bar{F}$ from the $\int d\hat{\mathbf{k}}\, \Gamma^{(2)}_{\psi\psi}\, \bar{\psi}_M(\hat{\mathbf{k}}) \bar{\psi}_M(-\hat{\mathbf{k}})$ and $\int d\hat{\mathbf{k}}\, \Gamma^{(2)}_{\psi c}\, \bar{\psi}_M(\hat{\mathbf{k}}) \bar{c}_M(-\hat{\mathbf{k}})$ terms of Eq. (B1) originating from the q^2 order term in $\bar{\psi}_M(\hat{\mathbf{k}})$. However since those terms are proportional to k^2 we do not need them to calculate $a_3(f)$.

In order to calculate the coefficients $a_2(f)$ and $a_3(f)$ in Eq. (23) we need to collect the terms in Eq. (B1) and Eq. (B2) which are proportional to $\ln(\xi^2)$. Thus $a_2(f)$ is proportional to

$$\left(\frac{3m}{V} \Gamma^{(3)}_{ccc}(\mathbf{0}, \mathbf{0}) + \frac{6m^2}{V^2} \Gamma^{(4)}_{cccc}(\mathbf{0}, \mathbf{0}, \mathbf{0}) \right) \int d\hat{\mathbf{k}}\, \bar{c}_M(\hat{\mathbf{k}}) \bar{c}_M(-\hat{\mathbf{k}}) \tag{B3}$$

and $a_3(f)$ is proportional to

$$\left(\Gamma^{(3)}_{ccc}(\mathbf{0}, \mathbf{0}) + \frac{4m}{V} \Gamma^{(4)}_{cccc}(\mathbf{0}, \mathbf{0}, \mathbf{0}) \right) \int d\hat{\mathbf{k}}_1 d\hat{\mathbf{k}}_2\, \bar{c}_M(\hat{\mathbf{k}}_1) \bar{c}_M(\hat{\mathbf{k}}_2) \bar{c}_M(-\hat{\mathbf{k}}_1 - \hat{\mathbf{k}}_2) \tag{B4}$$

The coefficient $b_2(f)$ is calculated from the part proportional to ξ^{-2} in Eq. (B2) which is

$$\left(\frac{3m}{V}\,\Gamma^{(3)''}_{ccc}(\mathbf{0},\mathbf{0}) + \frac{6m^2}{V^2}\,\Gamma^{(4)''}_{cccc}(\mathbf{0},\,\mathbf{0},\,\mathbf{0})\right)\int đ\,\hat{\mathbf{k}}\,(\hat{\mathbf{k}}\cdot\hat{\mathbf{k}})\bar{c}_M(\hat{\mathbf{k}})\bar{c}_M(-\hat{\mathbf{k}}) + \left(\Gamma^{(2)}_{\psi c}(\mathbf{0}) + \frac{2m}{V}\Gamma^{(3)}_{\psi cc}(\mathbf{0},\mathbf{0})\right.$$
$$\left. + \frac{3m^2}{V^2}\,\Gamma^{(4)}_{\psi ccc}(\mathbf{0},\,\mathbf{0},\,\mathbf{0})\right)\int đ\,\hat{\mathbf{k}}\,\bar{c}_M(\hat{\mathbf{k}})\bar{\psi}_M(-\hat{\mathbf{k}}) \tag{B5}$$

In the above expression the double prime in the superscript denotes second derivative with respect to $\hat{\mathbf{k}}$, *i.e.*, $f''(\mathbf{0}) = \partial^2 f(\hat{\mathbf{k}})/\partial\hat{\mathbf{k}}^2|_{\hat{\mathbf{k}}=0}$. $b_3(f)$ can be calculated from the part proportional to ξ^{-2} in Eq. (B2). However we will not need $b_3(f)$ to calculate ξ^{-2} to order $O(\epsilon)$, hence the calculation will not be shown here.

2. $\hat{\mathbf{k}} \to \mathbf{0}$ limit of the Γ functions

The $\hat{\mathbf{k}} \to 0$ limit of the $\Gamma^{(2)}$ functions are the following :

$$\Gamma^{(2)}_{\psi\psi}(\hat{\mathbf{k}}) \to \frac{9V}{2mNl_0^2 f^2(1-f)^2(\hat{\mathbf{k}}\cdot\hat{\mathbf{k}})} + \frac{(2f^2-2f+5)V}{8mf^2(1-f)^2} - \frac{\mu^2 V}{2m}$$
$$-vN^2\sum_{\alpha=0}^{n}\chi^\alpha \prod_{\beta=0,\beta\neq 0}^{n}\delta_{\mathbf{k}^\beta,0} + O((\hat{\mathbf{k}}\cdot\hat{\mathbf{k}})) \tag{B6}$$

$$\Gamma^{(2)}_{\psi c}(\hat{\mathbf{k}}) \to \frac{V(1-2f)}{4mf(1-f)} - \frac{V(4f^3-6f^2+8f-3)Nl_0^2(\hat{\mathbf{k}}\cdot\hat{\mathbf{k}})}{288mf(1-f)} - \frac{Vf\mu^2}{m}$$
$$+N^2\sum_{\alpha=0}^{n}u^\alpha \prod_{\beta=0,\beta\neq\alpha}^{n}\delta_{\mathbf{k}^\beta,0} + O((\hat{\mathbf{k}}\cdot\hat{\mathbf{k}})^2) \tag{B7}$$

$$\Gamma^{(2)}_{cc}(\hat{\mathbf{k}}) \to \frac{V}{2m} - \frac{Vf^2\mu^2}{2m} + \frac{(4f^2-4f+9)Nl_0^2(\hat{\mathbf{k}}\cdot\hat{\mathbf{k}})}{288m} + N^2\sum_{\alpha=0}^{n}w^\alpha \prod_{\beta=0,\beta\neq\alpha}^{n}\delta_{\mathbf{k}^\beta,0} + O((\hat{\mathbf{k}}\cdot\hat{\mathbf{k}})^2) \tag{B8}$$

Calculation of higher order Γ functions involve evaluation of higher order correlation functions in $\hat{\mathbf{r}}_i$'s. We will not show the detailed calculations here but will present the calculation of $\Gamma^{(3)}_{ccc}$ as an example ; the other Γ functions can be calculated in similar fashion.

$$\Gamma^{(3)}_{ccc}(\hat{\mathbf{k}}_1,\hat{\mathbf{k}}_2) = -\frac{1}{3!V}\sum_{a,b,c=1}^{2}\sum_{a',b',c'=1}^{2} G^{(3)}_{abc}(\hat{\mathbf{k}}_1,\hat{\mathbf{k}}_2-\hat{\mathbf{k}}_1,-\hat{\mathbf{k}}_2)G^{-1}_{aa'}(\hat{\mathbf{k}}_1)G^{-1}_{bb'}(\hat{\mathbf{k}}_2-\hat{\mathbf{k}}_1)G^{-1}_{cc'}(-\hat{\mathbf{k}}_2)\tau_{a'}\tau_{b'}\tau_{c'}\,. \tag{B9}$$

In the above equation, $\tau_1 = f$, $\tau_2 = 1 - f$ and $G_{ab}(\hat{\mathbf{k}}) = \int_a ds_1 \int ds_2 \langle e^{i\hat{\mathbf{k}}\cdot(\hat{\mathbf{r}}(s_1)-\hat{\mathbf{r}}(s_2))}\rangle_0$ where $\langle\cdots\rangle_0$ implies average over polymer configurations with the Boltzmann weight $e^{-\beta H_0}$, where $\beta H_0 = \sum_{i=1}^{m} 3/(2Nl_0^2)\int_0^1 ds\,(d\hat{\mathbf{r}}_i/ds)^2$. The inverse $G^{-1}_{ab}(\hat{\mathbf{k}}) = (-1)^{a+b}G_{ba}(\hat{\mathbf{k}})/\det|G(\hat{\mathbf{k}})|$. The function $G^{(3)}_{abc}(\hat{\mathbf{k}}_1, \hat{\mathbf{k}}_2 - \hat{\mathbf{k}}_1, -\hat{\mathbf{k}}_2)$ is given by,

$$
\begin{aligned}
G^{(3)}_{abc}(\hat{\mathbf{k}}_1, \hat{\mathbf{k}}_2 - \hat{\mathbf{k}}_1, -\hat{\mathbf{k}}_2) &= m\int_a ds_1 \int_b ds_2 \int_c ds_3 \left\langle \exp\left[i\hat{\mathbf{k}}_1\cdot\hat{\mathbf{r}}(s_1) + i(\hat{\mathbf{k}}_2 - \hat{\mathbf{k}}_1)\cdot\hat{\mathbf{r}}(s_2) - i\hat{\mathbf{k}}_2\cdot\hat{\mathbf{r}}(s_3)\right]\right\rangle_0 \\
&= m\int_a ds_1 \int_b ds_2 \int_c ds_3 \exp\left[-\frac{Nl_0^2}{6}\left\{ k_1^2|s_2 - s_1| + k_2^2|s_3 - s_2|\right\}\right] \\
&= m\int_a ds_1 \int_b ds_2 \int_c ds_3 \left(1 - \frac{Nl_0^2}{6}\left\{ k_1^2|s_2 - s_1| + k_2^2|s_3 - s_2|\right\} + O(k_1^4, k_2^4, k_1^2k_2^2)\right)
\end{aligned}
\tag{B10}
$$

A systematic diagrammatic way of calculating the G functions can be found in Ref. [39]. Since we are interested in the k^0 and k^2 terms in the Γ functions we will expand the G functions and collect the terms proportional to k^0 and k^2. Using the above equations we get

$$
\Gamma^{(3)}_{ccc}(\hat{\mathbf{k}}_1, \hat{\mathbf{k}}_2) = -\frac{V^2}{6m^2}\left[\frac{8f^3 - 4f^2 - 10f^2 + 29}{24} - \frac{4f^2 - 4f + 9}{24}\left\{\frac{Nl_0^2k_1^2}{6} + \frac{Nl_0^2k_2^2}{6}\right\}\right] + O(k_1^4, k_2^4, k_1^2k_2^2)
\tag{B11}
$$

3. $\bar{\psi}_M(\hat{\mathbf{k}})$ in the limit $\hat{\mathbf{k}} \to \mathbf{0}$

Using Eq. (B7) and Eq.(B8) we obtain

$$
\frac{\Gamma_{c\psi}(\hat{\mathbf{k}})}{\Gamma_{\psi\psi}(\hat{\mathbf{k}})} \to (1 - 2f - f\mu^2)f(1-f)Nl_0^2k^2 + O(k^4)
\tag{B12}
$$

Thus

$$
\bar{\psi}_M(\hat{\mathbf{k}}) \to [-qm(1 - 2f - f\mu^2)f(1-f)Nl_0^2k^2 + O(k^4)]\left(1 - \sum_{\alpha=0}^{n}\prod_{\beta=0,\beta\neq\alpha}^{n}\delta_{\mathbf{k}^\beta,0}\right)(1 - \delta_{\hat{\mathbf{k}},0})\,.
\tag{B13}
$$

4. Replica Integrals

All the replica integrals are evaluated in the limit $n \to 0$. The integral,

$$\begin{aligned} I_1 &= \int đ\hat{\mathbf{k}}\, \bar{c}_M(\hat{\mathbf{k}})\bar{c}_M(-\hat{\mathbf{k}}) \\ &= m^2q^2 \int đ\hat{\mathbf{k}}\, \delta_{\mathbf{k}_S\,0}\, e^{-2\hat{\mathbf{k}}^2\xi^2} - m^2q^2/V \\ &= m^2q^2 \int đ\hat{\mathbf{k}} \int \frac{d\mathbf{a}}{V}\, e^{i\mathbf{a}\cdot\mathbf{k}_S - 2\hat{\mathbf{k}}^2\xi^2} - m^2q^2/V \\ &= m^2q^2 \int \frac{d\mathbf{a}}{V} \left(\frac{1}{2\sqrt{2\pi}\xi}\right)^{3(n+1)} e^{-\mathbf{a}^2(n+1)/8\xi^2} - m^2q^2/V \\ &= \frac{m^2q^2}{V^n} \left(\frac{V^{1/3}}{2\sqrt{2\pi}\xi}\right)^{3(n+1)} \left(\frac{8\pi\xi^2}{(n+1)V^{2/3}}\right)^{3/2} - m^2q^2/V \\ &= -\frac{3m^2q^2}{2V} n \ln(8\pi\xi^2 V^{-2/3}) + O(n^2) \end{aligned} \tag{B14}$$

The integral

$$\begin{aligned} I_2 &= \int đ\hat{\mathbf{k}}_1\, đ\hat{\mathbf{k}}_2\, \bar{c}_M(\hat{\mathbf{k}}_1)\bar{c}_M(\hat{\mathbf{k}}_2)\bar{c}_M(-\hat{\mathbf{k}}_1 - \hat{\mathbf{k}}_2) \\ &= m^3q^3 \int đ\hat{\mathbf{k}}_1\, đ\hat{\mathbf{k}}_2\, \delta_{\mathbf{k}_{1S}\,0}\, \delta_{\mathbf{k}_{2S}\,0}\, e^{-(\hat{\mathbf{k}}_1^2 + \hat{\mathbf{k}}_2^2 + (\hat{\mathbf{k}}_1+\hat{\mathbf{k}}_2)^2)\xi^2} - \frac{3m^3q^3}{V} \int đ\hat{\mathbf{k}}_1 \delta_{\mathbf{k}_{1S}\,0}\, e^{-2\hat{\mathbf{k}}_1^2\xi^2} \\ &\quad + \frac{3q^3}{V} \int đ\hat{\mathbf{k}}_1 \delta_{\mathbf{k}_{1S}\,0}\, e^{-\hat{\mathbf{k}}_1^2\xi^2} - m^3q^3/V^2 \end{aligned} \tag{B15}$$

The second and third integral in the last line can be evaluated using Eq.(B14). We calculate the first integral here.

$$\begin{aligned} &\int đ\hat{\mathbf{k}}_1\, đ\hat{\mathbf{k}}_2\, \delta_{\mathbf{k}_{1S}\,0}\, \delta_{\mathbf{k}_{2S}\,0}\, e^{-(\hat{\mathbf{k}}_1^2 + \hat{\mathbf{k}}_2^2 + (\hat{\mathbf{k}}_1+\hat{\mathbf{k}}_2)^2)\xi^2} \\ &= \int đ\hat{\mathbf{k}}_1 đ\hat{\mathbf{k}}_2 \int \frac{d\mathbf{c}_1}{V}\frac{d\mathbf{c}_2}{V}\, e^{-(\hat{\mathbf{k}}_1^2\xi^2 + \hat{\mathbf{k}}_2^2\xi^2 + (\hat{\mathbf{k}}_1+\hat{\mathbf{k}}_2)^2\xi^2)} e^{i\mathbf{c}_1\cdot\hat{\mathbf{k}}_{+S} + i\mathbf{c}_2\cdot\hat{\mathbf{k}}_{-S}} \\ &= \left(\frac{1}{8\pi\xi^2}\right)^{3(n+1)/2} \int \frac{d\mathbf{c}_1}{V}\frac{d\mathbf{c}_2}{V} \int đ\hat{\mathbf{k}}_1\, \exp\left(-\frac{3\xi^2}{2}\hat{\mathbf{k}}_1^2 + i\hat{\mathbf{k}}\cdot(\mathbf{c}_1 + \mathbf{c}_2/2)\right) \\ &= \left(\frac{1}{48\pi^2\xi^4}\right)^{3(n+1)/2} \int \frac{d\mathbf{c}_1}{V}\frac{d\mathbf{c}_2}{V}\, \exp\left(-\frac{(n+1)c_1^2}{6\xi^2} - \frac{(n+1)c_2^2}{6\xi^2} - \frac{(n+1)\mathbf{c}_1\cdot\mathbf{c}_2}{6\xi^2}\right) \\ &= \frac{1}{V^2(n+1)^{3/2}} \left(\frac{V^{4/3}}{48\pi^2\xi^4}\right)^{3n/2} \\ &= 1/V^2 - 3n/V^2 \ln(4\sqrt{3}\pi\xi^2 V^{-2/3}) + O(n^2) \end{aligned} \tag{B16}$$

Thus

$$I_2 = -\frac{3m^3q^3n}{V^2}\left(\ln(4\sqrt{3}\pi\xi^2V^{-2/3}) - \frac{3}{2}\ln 2\right) + O(n^2) \tag{B17}$$

The integral

$$\begin{aligned}
I_3 &= \int đ\hat{\mathbf{k}}\,(\hat{\mathbf{k}}\cdot\hat{\mathbf{k}})\,\bar{c}_M(\hat{\mathbf{k}})\bar{c}_M(-\hat{\mathbf{k}}) \\
&= q^2m^2\int\frac{d\mathbf{a}}{V}\int đ\hat{\mathbf{k}}\left(\sum_{\alpha=0}^{n}(k^\alpha)^2\right)\prod_{\alpha=0}^{n}\left(e^{i\mathbf{k}^\alpha\cdot\mathbf{a}-2(k^\alpha)^2\xi^2}\right) \\
&= q^2m^2\int\frac{d\mathbf{a}}{V}\int\left(\prod_{\alpha=0}^{n}\frac{dk^\alpha(k^\alpha)^2}{(2\pi)^3}d\phi d\theta^\alpha\sin(\theta^\alpha)e^{ik^\alpha a\cos(\theta^\alpha)-2(k^\alpha)^2\xi^2}\right)\left(\sum_{\alpha=0}^{n}(k^\alpha)^2\right) \\
&= q^2m^2\int\frac{d\mathbf{a}}{V}\,a^{-(n+1)}\int\left(\prod_{\alpha=0}^{n}\frac{dk^\alpha}{(2\pi)^2}(k^\alpha)2\sin(k^\alpha a)e^{-2(k^\alpha)^2\xi^2}\right)\left(\sum_{\alpha=0}^{n}(k^\alpha)^2\right) \\
&= 2(n+1)q^2m^2\int\frac{d\mathbf{a}}{V}\,a^{-(n+1)}\int\frac{dk^0(k^0)^3}{2\pi}\sin(k^0a)e^{-2(k^0)^2\xi^2}\int\left(\prod_{\alpha=1}^{n}\frac{dk^\alpha k^\alpha}{2\pi}2\sin(k^\alpha a)e^{-2(k^\alpha)^2\xi^2}\right) \\
&= \frac{3(n+1)(4\pi)^{-3/2(n+1)}q^2m^2}{2(2\xi^2)^{(3n+5)/2}}\int\frac{d\mathbf{a}}{V}\,e^{-a^2(n+1)/8\xi^2}\,{}_1F_1(-1;3/2;a^2/8\xi^2)\left({}_1F_1(0;3/2;a^2/8\xi^2)\right)^n \\
&= \frac{3(n+1)(4\pi)^{-3/2(n+1)}q^2m^2}{2(2\xi^2)^{(3n+5)/2}}\int\frac{d\mathbf{a}}{V}\,e^{-a^2(n+1)/8\xi^2}\,{}_1F_1(-1;3/2;a^2/8\xi^2)\,(1+O(n)) \\
&= \frac{3(n+1)(4\pi)^{-1/2(3n+1)}q^2m^2}{2(2\xi^2)^{(3n+5)/2}}\int_0^\infty\frac{da}{V}\,a^2\,e^{-a^2(n+1)/8\xi^2}\,{}_1F_1(-1;3/2;a^2/8\xi^2)\,(1+O(n)) \\
&= \frac{3(n+1)(4\pi)^{-3n/2}q^2m^2}{2V(2\xi^2)^{(3n+2)/2}}\frac{n}{1+n}\,(1+O(n)) \\
&= \frac{3nq^2m^2}{4V\xi^2} + O(n^2)
\end{aligned} \tag{B18}$$

The expansion $\lim_{n\to 0}x^n = 1 + n\ln(x) + n^2/2(\ln(x))^2 + O(n^3)$ and the integrals [69] for hypergeometric functions [68] have been used in the above derivation.

The integral,

$$\begin{aligned}
I_4 &= \int đ\hat{\mathbf{k}}\,c_M(\hat{\mathbf{k}})\psi_M(-\hat{\mathbf{k}}) \\
&= -m^2q^2\int đ\hat{\mathbf{k}}\,\delta_{\mathbf{k}_S\,0}\,\frac{(\Gamma^{(2)}_{\psi c}(\hat{\mathbf{k}}))^2}{\Gamma^{(2)}_{\psi\psi}(\hat{\mathbf{k}})}\,e^{-2\hat{\mathbf{k}}^2\xi^2}
\end{aligned} \tag{B19}$$

In the limit $\xi\to\infty$ the significant contribution comes from $k\sim 1/\xi\to 0$. Therefore one can expand

$$\frac{(\Gamma^{(2)}_{\psi c}(\hat{\mathbf{k}}))^2}{\Gamma^{(2)}_{\psi\psi}(\hat{\mathbf{k}})} = V\left\{\frac{1-2f}{4mf(1-f)} - \frac{\mu^2 f}{m}\right\}^2\frac{2}{9}Nf^2(1-f)^2ml_0^2(\hat{\mathbf{k}}\cdot\hat{\mathbf{k}})(1+O((\hat{\mathbf{k}}\cdot\hat{\mathbf{k}}))) \tag{B20}$$

Thus we can use the integral in Eq. (B6) to evaluate the $(\hat{\mathbf{k}}\cdot\hat{\mathbf{k}})$ part of the integral.

5. Calculation of $a_2(f)$, $a_3(f)$ and $b_2(f)$

We can calculate the coefficients in Eq. (23) using the results from the last sections.

$$a_2(f) = 0 \tag{B21}$$

$$a_3(f) = \frac{1}{2} \tag{B22}$$

$$b_2(f) \;=\; \frac{(1-2f)^2(24f^3-36f^2-46f+29)}{55296f(1-f)} + \frac{4f^2-4f+9}{288} \tag{B23}$$

In experiments $f = 0.25$ where $a_2 = 0$, $a_3 = 1/2$ and $b_2(0.25) = 0.028$.

APPENDIX C: CALCULATION OF A_2

In order to calculate A_2 in Eq. (25) to order q^2/ξ^2 we can Taylor expand $\Gamma^{(4)}_{\psi\psi cc}(\mathbf{k}^\alpha, \hat{\mathbf{k}}', -\hat{\mathbf{k}}')$ around $\hat{\mathbf{k}}' = 0$ upto order $\hat{\mathbf{k}}'\cdot\hat{\mathbf{k}}'$. Since $\psi_M(\hat{\mathbf{k}}') \propto q\,\hat{\mathbf{k}}'\cdot\hat{\mathbf{k}}'$ we do not need to consider the second term in Eq. (25) in the calculation of A_2 till $O(q^2/\xi^2)$.

$$A_2(\mathbf{k}^\alpha) = \frac{1}{V}\int đ\hat{\mathbf{k}}' \left[\Gamma^{(4)}_{\psi\psi cc}(\mathbf{k}^\alpha, \mathbf{0}, \mathbf{0}) + \frac{1}{2}\Gamma''^{(4)}_{\psi\psi cc}(\mathbf{k}^\alpha, \mathbf{0}, \mathbf{0})(\hat{\mathbf{k}}'\cdot\hat{\mathbf{k}}')\right]\bar{c}_M(\hat{\mathbf{k}}')\bar{c}_M(-\hat{\mathbf{k}}') \tag{C1}$$

Since the phase separation occurs at the length scale of k_m^{-1} we calculate A_2 at $k = k_m = (108/(f(1-f)N^2 l_0^4))^{1/4}$.

$$A_2(k_m) = \frac{q^2 V}{m}(t_0(k_m, f)\ln(\xi^2) + t_1(k_m, f)/\xi^2) \tag{C2}$$

From our calculations $t_0(k_m, 0.25) = 1.115$ and $t_1(k_m, 0.25) = 0.212$.

Table 1

Sample	DCP (wt %)	Swelling ratio (ϕ)	N_c,[a] (perchain)	N_c^{FE},[b]
SI[0.00]	0	∞[c]	0	N/A[c]
SI[0.40]	0.4	∞[c]	0.95	N/A[c]
SI[0.65]	0.65	0.0485	1.53	2.35
SI[0.70]	0.70	0.0367	1.65	2.23
SI[1.06]	1.06	0.0748	2.40	2.73
SI[1.16]	1.16	0.0833	2.73	2.89
SI[1.58]	1.58	0.1386	3.71	4.33
SI[1.94]	1.94	0.1464	4.56	4.5
SI[4.06]	4.06	0.2620	9.54	11.3

a. Calculated based on stoichiometric ratio of DCP to SI block copolymer.

b. Calculated based on swelling equilibrium results and F-E theory.

c. Sample disassembled when placed in excess toluene.

[1] Doi, M. *Introduction to Polymer Physics*, Oxford, NY, 1997.

[2] Leibler, L. *Macromolecules*, **1980**, 13, 1602.

[3] Fetters, L. J.; Morton, M. *Macromolecules* **1969**, 2, 453.

[4] Frick, E. M.; Zalusky, A. S.; Hillmyer, M. A. *Biomolecules* **2003**, 4, 216.

[5] Holden, G.; Legge, N. R.; Quirk, R. P.; Schroeder, H. E. *Thermoplastic Elastomer*, 2nd ed.; Hanser/Gardner: Cincinnati, 1993

[6] Yu, J. M.; Dubois, P.; Jerome, R. *Macromolecules* **1996**, 29, 7316.

[7] Finkelman, H.; Kundler, I.; Terentjev, E.; Warner, M. *J. Phys. II France* **1997**, 7, 1059.

[8] Lendlein, A.; Langer, R. *Science* **2002**, 296, 1673.

[9] Irie, M. *Shape Memory Polymers*; Cambridge University Press: Cambridge, UK, 1998.

[10] Liu, C.; Chun, S. B.; Mather, P. T.; Zheng, L.; Haley, E. H.; Coughlin,E. B. *Macromolecules* **2002**, 35, 9868.

[11] Katchalsky, A. *Experientia* **1949**, 5, 319.

[12] Tanaka, T. *Phy. Rev. Lett.* **1978**, 40, 820.

[13] Flory, P. J.; Erman, B. *Macromolecules* **1982**, 15, 800.

[14] deGennes, P. G. C. R. *Acad. Sci. Paris* **1997**, t324, 343.

[15] Thurnmond, K. B.; Kowaleski, T.; Wooley, K. L. *J. Am. Chem. Soc.* **1996**, 118, 7239.

[16] Emoto, K.; Iijima, M.; Nagasaki, Y.; Kataoka, K. *J. Am. Chem. Soc.* **2000**, 122, 2653.

[17] Butun, V.; Billingham, N. C.; Armes, S. P. *J. Am. Chem. Soc.* **1998**, 120, 12135.

[18] Ding, J.; Liu, G. *Macromolecules* **1998**, 31, 6554.

[19] Zubarev, E. R.; Pralle, M. U.; Li, L.; Stupp, S. I. *Science* **1999**, 283, 523.

[20] Ding, J.; Liu, G. *J. Phys. Chem. B* **1998**, 102, 6107.

[21] Won, Y. Y.; Davis, H. T.; Bates, F. S. *Science* **1999**, 283, 960.

[22] Hillmyer, M. A.; Lipic, P. M.; Hajduk, D. A.; Almdal, K.; Bates, F. S. *J. Am. Chem. Soc.* **1997**, 119, 2749.

[23] Sakurai, S ; Twane, K. ; Nomura, S. *Macromolecules* **1993**, 26, 5479.

[24] Templin, M.; Franck, A.; Chesne, A. D.; Leist, H.; Zhang, Y.; Ulrich, R.; Schadler, V.; Wiesner, U. *Science* **1997**, 278, 1795.

[25] Golden, J. H.; DiSalvo, F. J.; Frechet, J. M. J.; Silcox, J.; Thomas, M.; Elman, J. *Science*

1996, 273, 782-784.

[26] Deam, R. T. and Edwards, S. F. *Phil. Trans. R. Soc. London A* **1975**, 280, 317.

[27] deGennes, P. G. *Scaling Concepts in Polymer Physics*, Cornell University Press, Ithaca, NY, 1986.

[28] Hahn, H.; Eitouni, H. B. ; Balsara, N. P.; Pople, J. A. *Phys. Rev. Lett.* **2003**, 90, 155505.

[29] Edwards, S. F. *Proc. Phys. Soc. London* **1965**, 85, 613.

[30] Doi, M. ; Edwards, S. F. *The Theory of Polymer Dynamics*, Clarendon Press, Oxford, 1986.

[31] Lin, C. C.; Jonnalagadda, S. V.; Kesani, P. K.; Dai, H. J.; Balsara, N. P. *Macromolecules* **1994**, 27, 7769.

[32] Gutin, A. M. ; Shakhnovich, E. I. *J. Chem. Phys.* **1994**, 100, 5290.

[33] Goldbart, P. M. ; Castillo, H. E. ; Zippelius, A. *Adv. Phys.* **1996**, 45, 393.

[34] Roos, C. ; Zippelius, A. ; Goldbart, P. M. *J. Phys. A*, **1997**, 30, 1967.

[35] Ball, R. C. ; Edwards, S. F. *Macromolecules* **1980**, 13, 748.

[36] Binder, K. ; Young, A. P. *Rev. Mod. Phys.* **1986**, 58, 801.

[37] Ohta, T. ; Kawasaki, K. *Macromolecules* **1986**, 19, 2621.

[38] Panyukov, S. ; Rabin, Y. *Phys. Rep.* **1996**, 269, 1.

[39] Qi, S. ; Chakraborty, A. K. *J. Chem. Phys.* **2001**, 115, 3386.

[40] Castillo, H. E. ; Goldbart, P. M. ; Zippelius, A. *Euro. Phys. Lett.* **1994**, 28, 519.

[41] The mean field second order transition at $f = 1/2$ for uncrosslinked copolymer melts becomes a weakly first order phase transition when fluctuations in the order parameter are accounted for [58]. Since the structure of F_1 is similar to the structure of the uncrosslinked copolymer system we expect the fluctuation effects to change the mean field second order transition at $f = 1/2$ into a weakly first order transition.

[42] The presence of the nonintensive $\ln(V^{-2/3})$ can be attributed [33] to the omission of the disorder average of the Gibbs symmetry factor. The difference in the standard Gibbs symmetry factor $1/(Nm)!$ in the cross-linked system arises since the cross-linked monomers are distinct from their uncrosslinked counterparts hence the standard Gibbs symmetry factor which treats all the monomers identically has to be modified. However the results in the paper which are extracted from the intensive part of the free energy will remain the same when those corrections are implemented.

[43] For homopolymers the value of N_c^* is changed from $1/2$ to $N_c^* \approx 0.8$ [44] if contributions from

the terms proportional to k^n when $n > 2$ are included in the free energy $\bar{F}$.

[44] Goldbart, P. M. ; Zippelius, A. *Phys. Rev. Lett.* **1993**, 71, 2256.

[45] Chaikin, P. M. ; Lubensky, T. *Principles of condensed matter physics*, Cambridge University Press, Cambridge, 1998.

[46] Balsara, N. P.; Perahia, D.; Safinya, C. R.; Tirrell, M.; Lodge, T. P. *Macromolecules* **1992**, 25, 3896.

[47] Queslel, J. P.; Mark, J. E. *J. Chem. Phys.* **1985**, 82, 3449.

[48] Queslel, J. P.; Mark, J. E. *Adv. Polym. Sci.* **1985**, 71, 229.

[49] Gundert, F; Wolf, B. A. In *Polymer Handbook*; 3rd ed; Brandrup, J. ; Immergut, E. H., Eds.; John Wiley and Sons, NY, 1989; p VII/173.

[50] Gonzalez, L.; Rodriguez, A.; Marcos, A.; Chamorro, C. *Rubber Chemistry and Technology* **1996**, 69, 203

[51] Ryan, A. J.; Hamley, I. W. In *The physics of glassy polymers* ; Haward, R. N.; Young, R. J., Eds.; Chapman and Hall: London, 1997.

[52] Schulz, M. F.; Khandpur, A. K.; Bates, F. S.; Almdal, K.; Mortensen, K.; Hajduk, D. A.; Gruner, S. M. *Macromolecules* **1996** , 29, 2857.

[53] Almdal, K.; Rosedale, J. H.; Bates, F. S.; Wignall, G. D.; Fredrickson, G. H. *Phys. Rev. Lett.* **1990**, 65, 1112.

[54] Bates, F. S.; Rosedale, J. H.; Fredrickson, G. H. *J. Chem. Phys.* **1990**, 92, 6255.

[55] Sakamoto, N.; Hashimoto, T. *Macromolecules* **1995**, 28, 6825.

[56] Stuhn, B.; Mutter, R.; Albrecht, T. *Europhys. Lett.* **1992**, 18, 427.

[57] Hashimoto, T.; Fujimura, M.; Kawai, H. *Macromolecules* **1980**, 13, 1660.

[58] Fredrickson, G. H.; Helfand, E. *J. Chem. Phys.* **1987**, 87, 697.

[59] Helfand, E.; Wasserman, Z. R. In *Developments in Block Copolymers*; Goodman, I., Ed.; Applied Science: London, 1982; Vol. 1.

[60] $\sqrt{4}k_m$ peak expected from a hexagonal lattice is suppressed by the cylinder form factor. The absence of the km peak is not unexpected and is often reported in the block copolymer literature [51, 61].

[61] Koppi, K. A.; Tirrell, M.; Bates, F. S.; Almdal, K.; Mortensen, K. *J. Rheo.* **1994**, 38, 999.

[62] Hanley, K. J.; Lodge, T. P. J. Polym. Sci. Polym. Phys. Ed. **1988**, 36, 3101.

[63] Rouf, C. ; Bastide, J. ; Pujol, J. M. ; Schosseler, F. ; Munch, J. P. *Phys. Rev. Lett.* **1994**, 73,

830.

[64] Shibayama, M. *Macromol. Chem. Phys.* **1998**, 199, 1.

[65] Warner, M.; Terentjev, E. *Prog. Polym. Sci.* **1996**, 21, 853.

[66] Mitchell, G. R.; Davis, F. J.; Guo, W.; Cywinski, R. *Polymer* **1991**, 32, 1347

[67] Finkelman, H.; Koch, H. J.; Rehage, G. *Makromol. Chem. Rapid Commun.* **1981**, 2, 317.

[68] Abramowitz, M. ; Stegun, I. A. in *Handbook of Mathematical Functions* Dover Publications, Inc., 5th Ed., NY, 1968.

[69] Gradshteyn, I. S. ; Ryzhik, I. M. *Table of Integrals, Series and Products*, 4th Ed. Academic Press, Inc. NY, 1992.

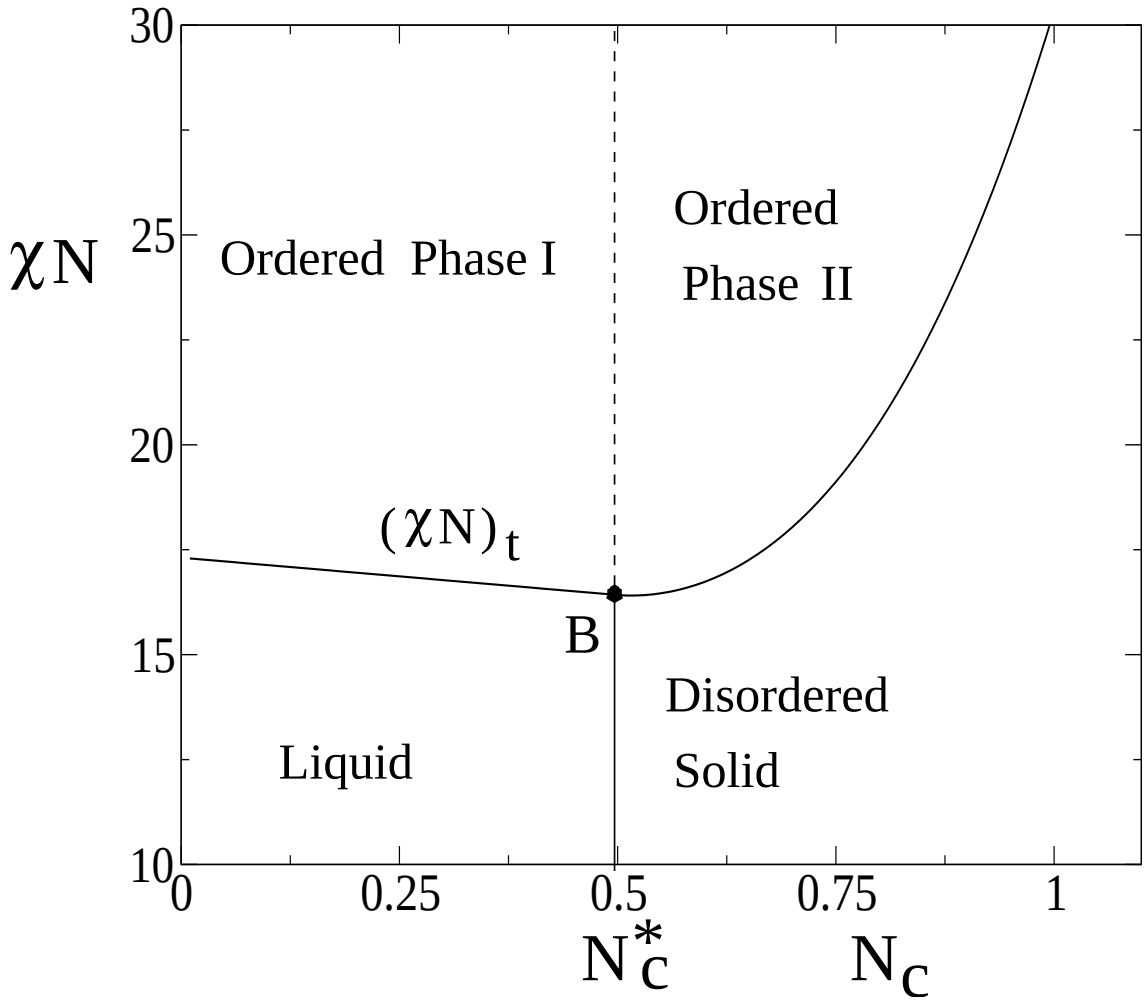

FIG. 1: The phase diagram in the $\chi N - N_c$ plane at $f = 0.25$, where N is the number of monomers in each chain, N_c is the average number of cross-links per chain, χ is the Flory-Huggins parameter and f is the volume fraction between A (PS) and B (PI) blocks in the copolymer chain. The curved line separating the disordered phases from the ordered phases is a plot of $(\chi N)_t$ vs N_c. The cross-linked melt undergoes a continuous transition across the solid line from the liquid phase to the disordered solid phase as N_c crosses N_c^* at where $\chi N < (\chi N)_t$. At $\chi N > (\chi N)_t$ the system changes continuously from an ordered phase in liquid matrix (ordered phase I) to an ordered phase in gel matrix (ordered phase II) as N_c increases above N_c^*. The phase transition from the disordered phase to the ordered state at a constant cross-link density N_c is first order. B is a bi-critical point.

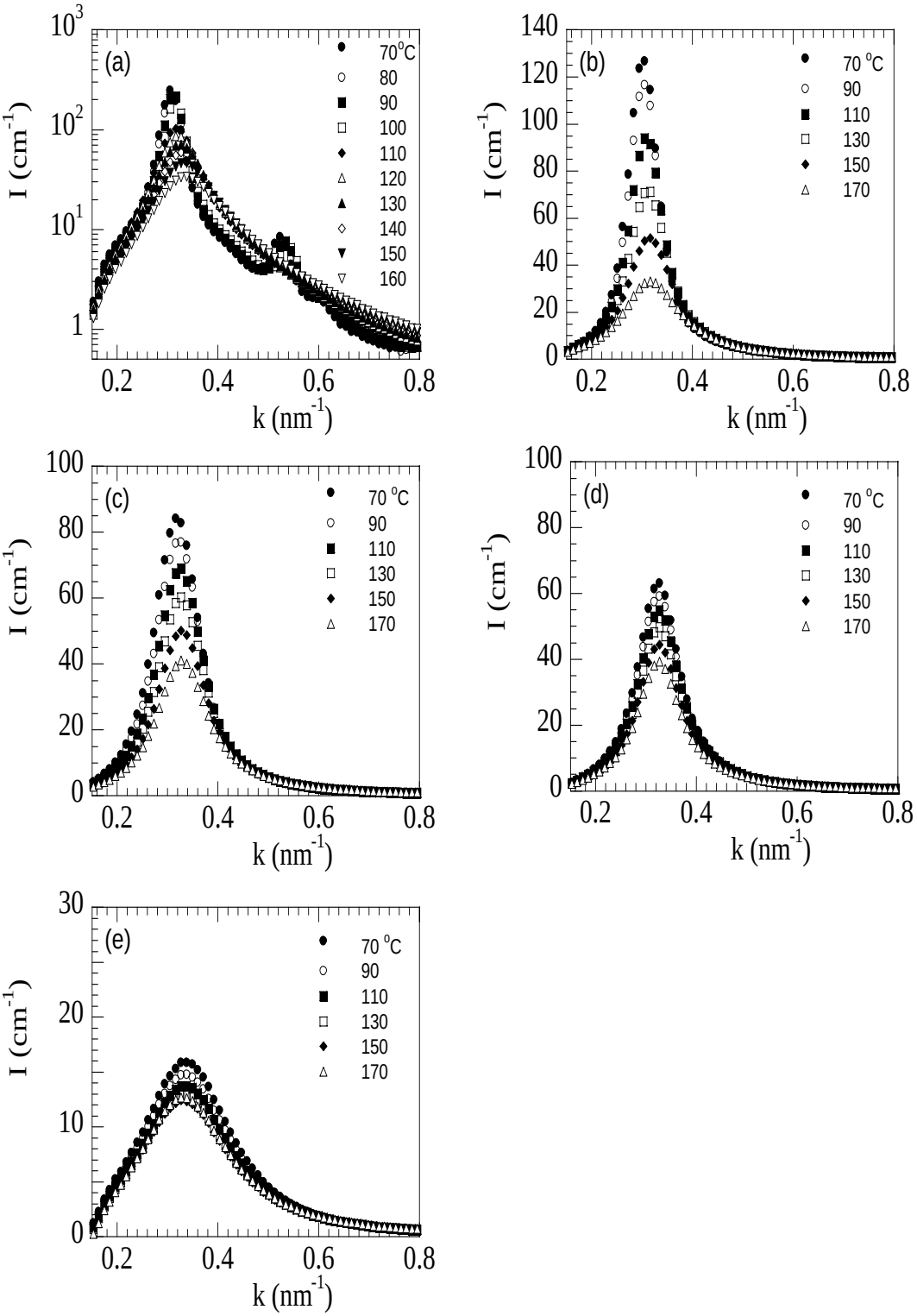

FIG. 2: SAXS intensity profile $I(k)$ as a function of scattering vector k for (a) SI[0.00] (b) SI[0.65] (c) SI[1.16] (d) SI[1.94] (e) SI[4.06] at various temperatures.

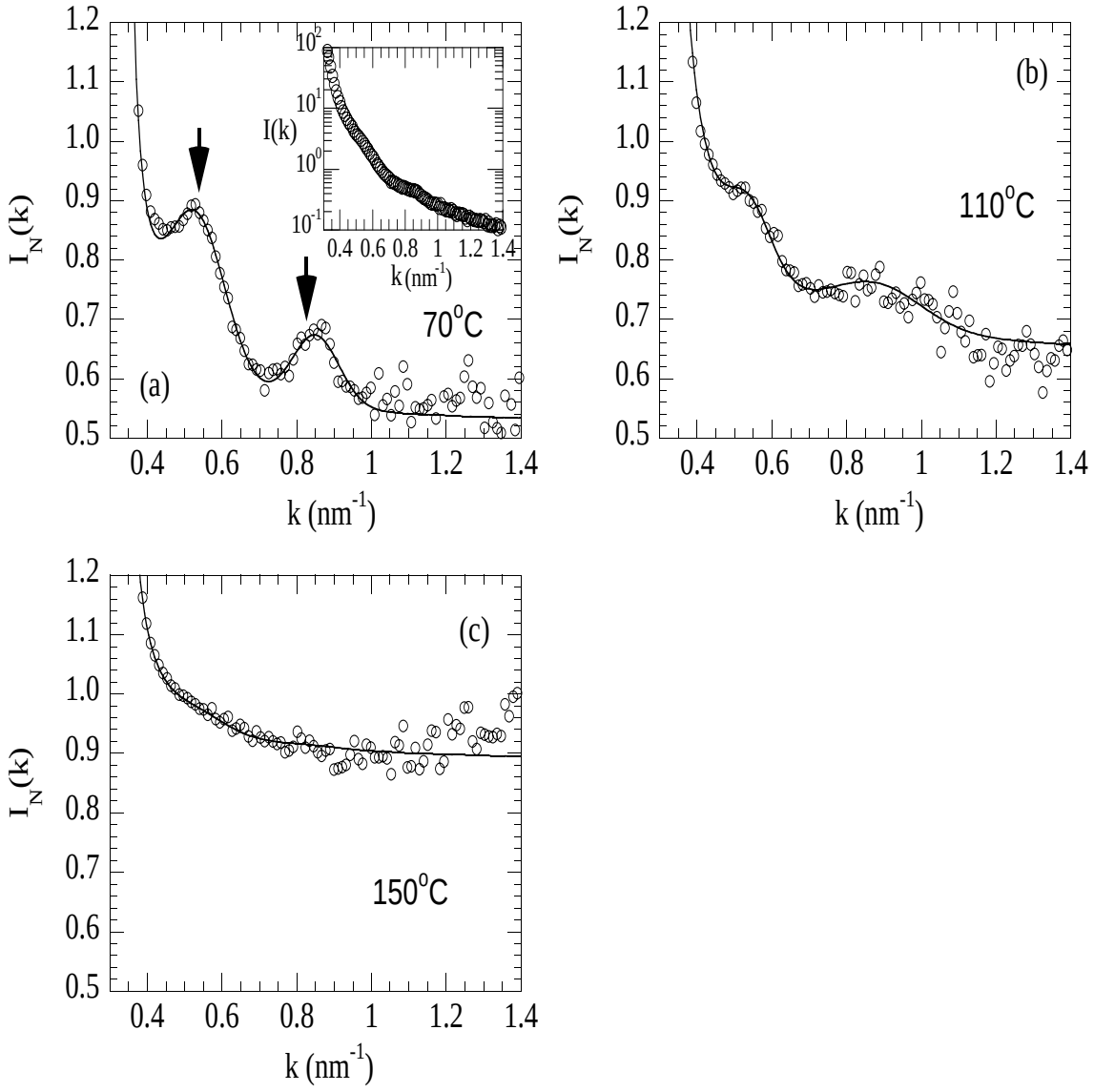

FIG. 3: Normalized SAXS intensity $I_N = I/[I \text{ at } T = 170°\text{C}]$ versus scattering vector $\mathbf{k}$ in the vicinity of the second order peak at selected temperatures (a) 70°C (b) 110°C (c) 150°C. Arrows mark higher order peaks at $\sqrt{3}k_m$ and $\sqrt{7}k_m$, where k_m is the position of the primary peak. Solid line represents least square fit of the data to the Eq. 35.

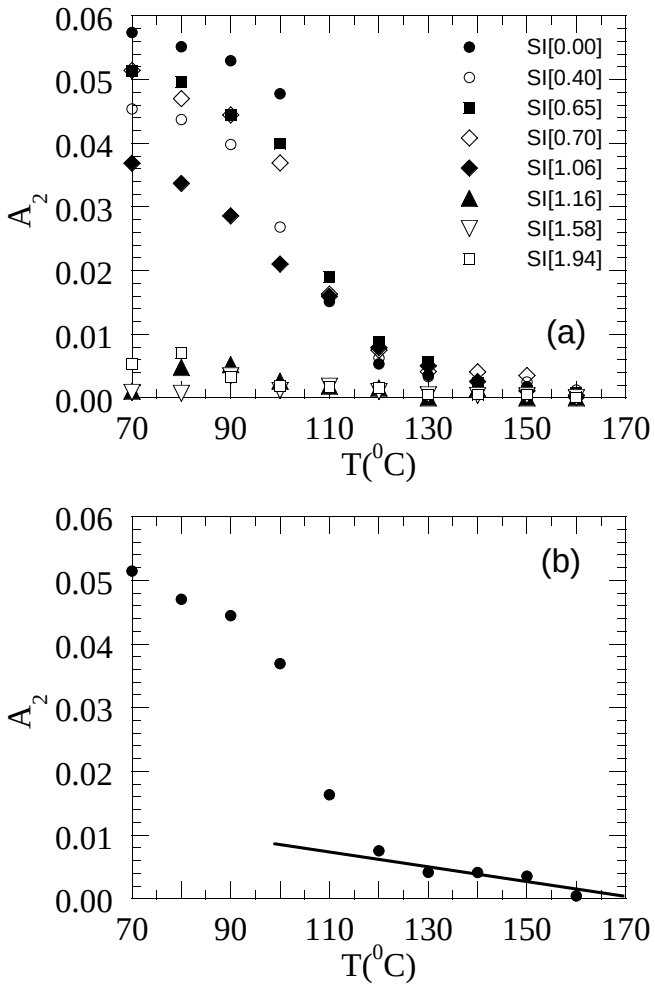

FIG. 4: (a) Temperature dependence of A_2, the area under the second order SAXS peak, obtained from cross-linked SI samples. (b) Temperature dependence of A_2 at SI[0.70]. Solid line is the least square fit through high temperature data ($T \geq 130^{\circ}$C). The order-disorder transition is marked by the first point of departure from this line at $T = 110^{\circ}$C.

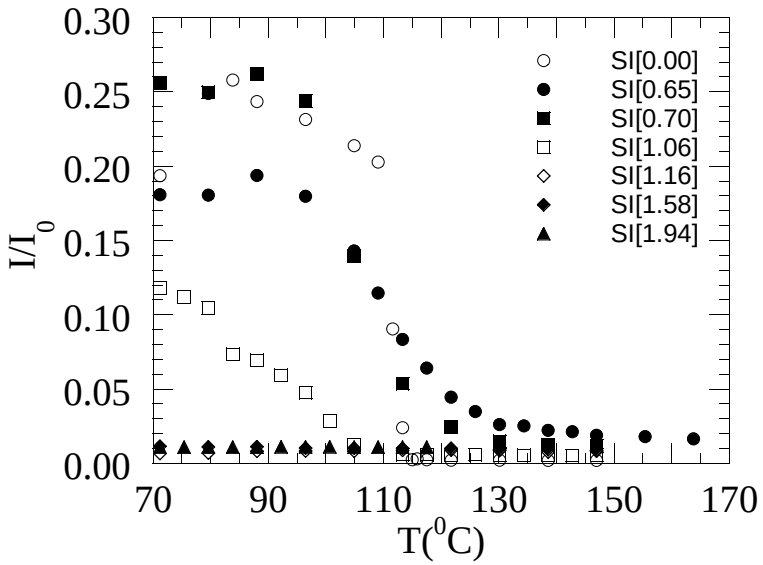

FIG. 5: Temperature dependence of the birefringence signal, I/I_0, from various DCP concentrations.

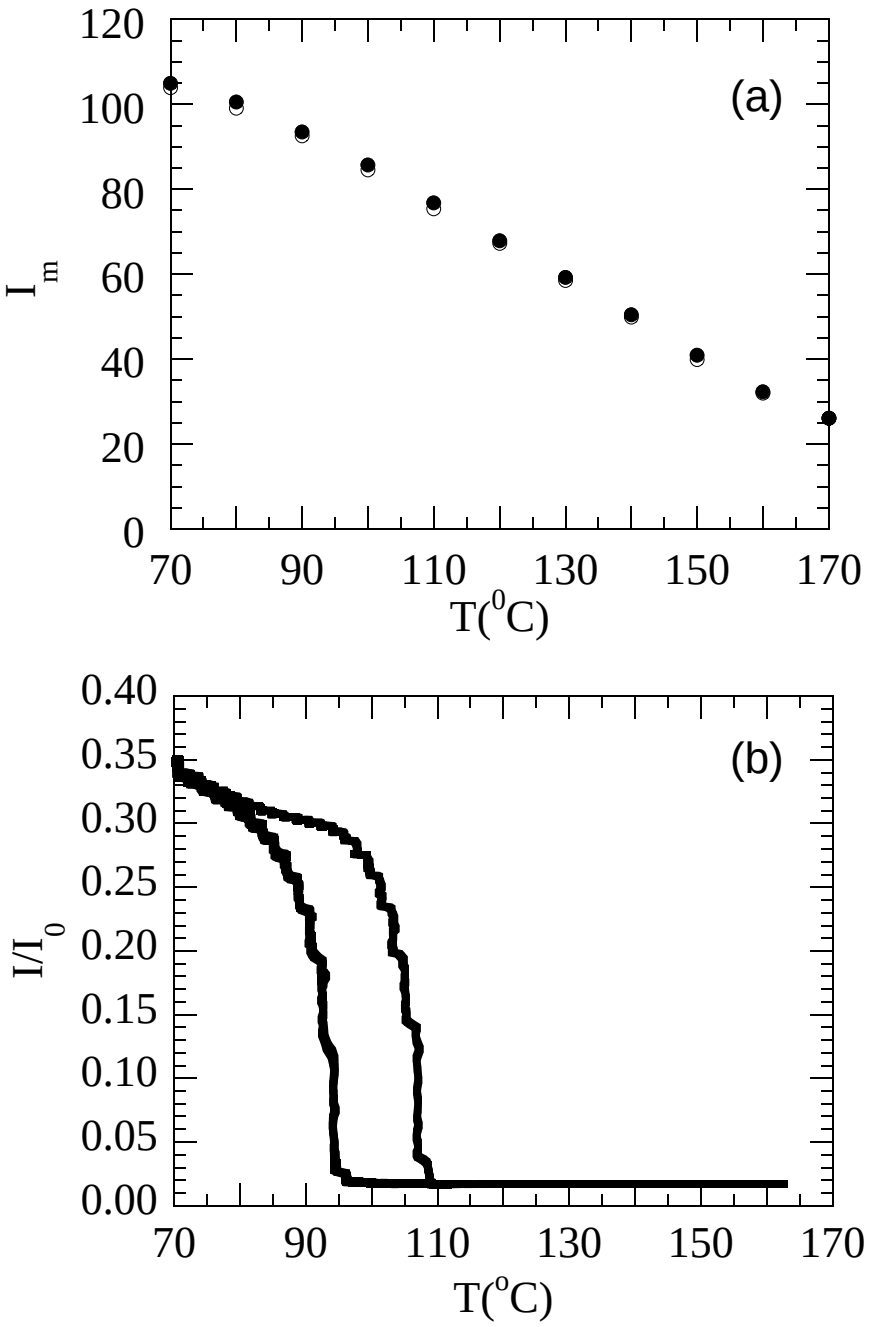

FIG. 6: Temperature dependence of (a) SAXS peak intensity, I_m during heating (•) and cooling (∘) (b) the birefringence, I/I_0, during a heating and cooling cycle of SI[0.70].

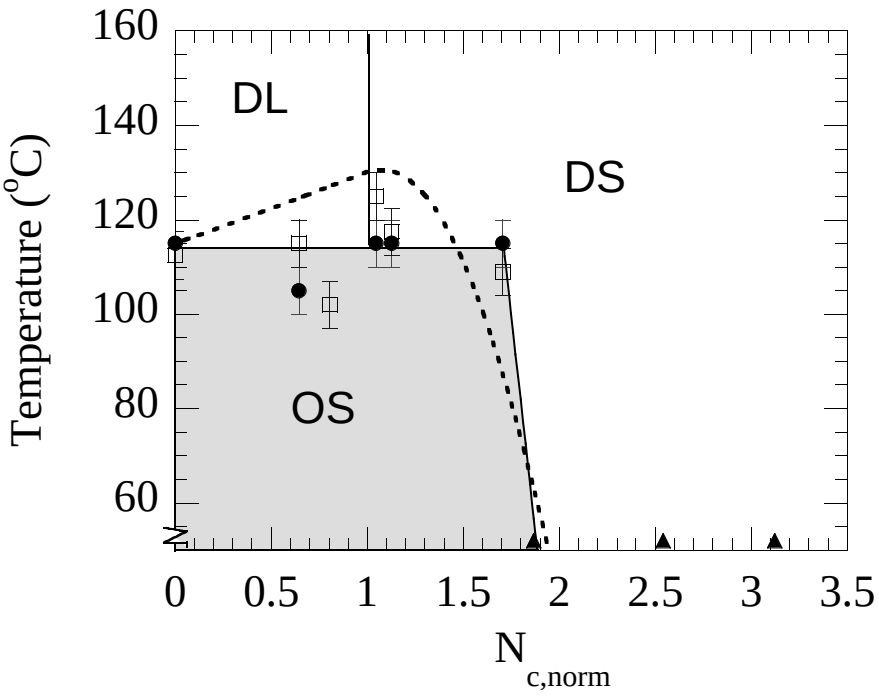

FIG. 7: Phase diagram cross-linked SI block copolymers, temperature versus the normalized number of cross-links per chain, $N_{c,norm}$. The solid line represents experimentally determined stability limit of each phase (disordered liquid : DL, ordered solid : OS, and disordered solid : DS). The dashed line represents the theoretically determined stability limit of the ordered solid. The symbols represent the order-disorder transition temperature, T_{ODT}, measured by birefringence (square) and SAXS (•). Triangles (filled △) represent samples with undetectable T_{ODT}, *i.e.* T_{ODT} was below 60°C, the glass transition temperature of the polystyrene microphase.